

LEAD: An EEG Foundation Model for Alzheimer’s Disease Detection

Yihe Wang¹ Nan Huang¹ Nadia Mammone² Marco Cecchi³ Xiang Zhang¹

Abstract

Electroencephalography (EEG) provides a non-invasive, highly accessible, and cost-effective approach for detecting Alzheimer’s disease (AD). However, existing methods, whether based on handcrafted feature engineering or standard deep learning, face three major challenges: 1) the lack of large-scale EEG-based AD datasets for robust representation learning; 2) limited generalizability across subjects; and 3) difficulty in adapting to highly heterogeneous data. To address these challenges, we curate the world’s largest EEG-AD corpus to date, comprising 2,238 subjects. Leveraging this unique resource, we propose LEAD, the first large-scale foundation model for EEG-based AD detection. Specifically, we design a gated temporal-spatial Transformer that can adapt to EEG recordings with arbitrary lengths, channel configurations, and sampling rates. In addition, we introduce a subject-regularized training strategy to enhance subject-level feature learning. We further employ medical contrastive learning for pre-training on 13 datasets, including 4 AD datasets and 9 non-AD neurological disorder datasets, and fine-tune/test the model on the other 5 AD datasets. LEAD achieves the best average ranking across all 20 evaluations on 5 downstream datasets, substantially outperforming existing approaches, including state-of-the-art (SOTA) EEG foundation models. These results strongly demonstrate the effectiveness and practical potential of the proposed method for real-world EEG-based AD detection. Source code: <https://github.com/DL4mHealth/LEAD>

¹Department of Computer Science, University of North Carolina at Charlotte, United States ²DICEAM Department, University Mediterranea of Reggio Calabria, Italy ³Cognition, Kentucky, United States. Correspondence to: Xiang Zhang <xiang.zhang@charlotte.edu>.

Table 1. Comparison of different AD detection technologies. CSF: Cerebrospinal Fluid.

Technologies	Accessibility↑	Safety↑	Affordability↑	Accuracy↑
CSF	Low	Low	Low	High
Neuroimaging	High	High	Low	High
Blood Test	Low	Moderate	Moderate	Moderate
Neurological Exam	High	High	Moderate	Moderate
EEG	High	High	High	Low

1. Introduction

Alzheimer’s Disease (AD) is the most common neurodegenerative disorder in the elderly, affecting 38 million individuals with \$1.3 trillion annual financial cost (Breijyeh & Karman, 2020; Masters et al., 2015; National Academies of Sciences, Engineering, and Medicine, 2021). Early detection of AD is a significant step to slow symptom progression and increase patients’ life expectancy (Nelson & Tabet, 2015; Chu, 2012). Compared with other AD detection modalities, electroencephalography (EEG) offers appealingly unique advantages (Table 1). These include high accessibility through portable devices, strong safety due to its non-invasive nature, and high affordability with low hardware and operational costs (Ieracitano et al., 2019a). In addition, EEG enables long-term monitoring of disease progression with high temporal resolution and real-time capability (Ahmed et al., 2025). Existing EEG-based AD detection methods generally fall into two main research directions. The first relies on handcrafted biomarkers, such as phase shift (Wang et al., 2017), power spectral density (Fahimi et al., 2017), and Shannon entropy (Azami et al., 2019). The second direction leverages deep learning models, including convolutional neural networks (Roncero-Parra et al., 2024), graph neural networks (Klepl et al., 2023), and Transformer-based architectures (Wang et al., 2024c). Detailed review of these approaches in the Related Work section and Appendix A.

However, existing EEG-based AD detection methods, whether using manual feature extraction or deep learning, still suffer from several limitations. First, large and high-quality datasets remain scarce. The cost and complexity of collecting EEG data from patients with AD result in most studies being conducted on relatively small cohorts, typically ranging from 20 to 100 subjects, and evaluated on a single dataset (Aviles et al., 2024). The limited diversity and scale of existing EEG datasets pose a fundamental challenge to learn robust models. Second, model generalizability across subjects remains a critical bottleneck. The core chal-

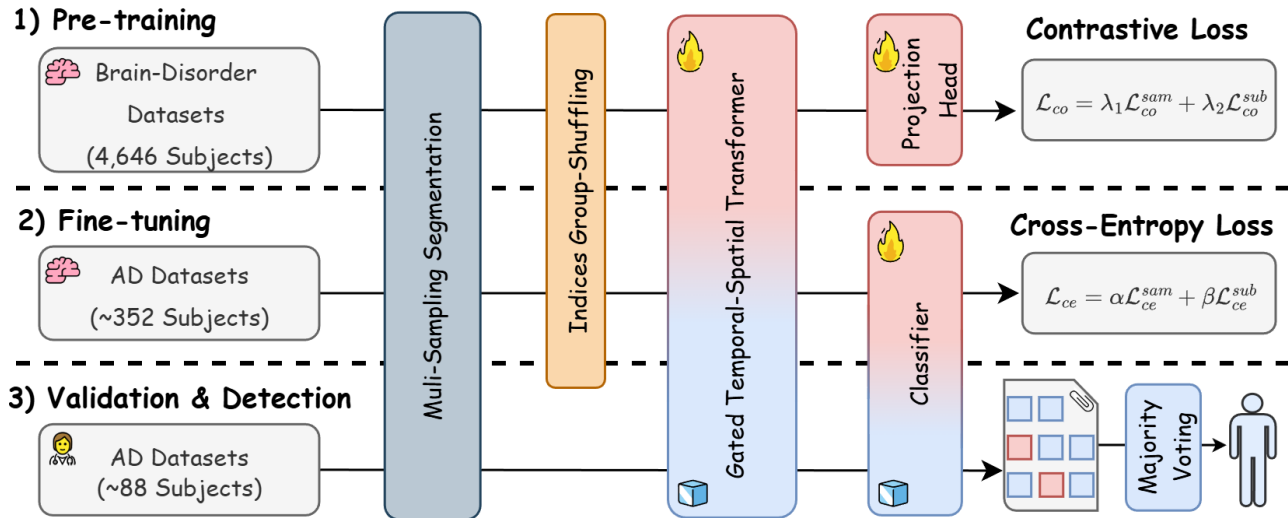


Figure 1. LEAD overview. We pre-train LEAD on 13 datasets of neurological disorders using medical contrastive learning. The model is then fine-tuned on 5 AD datasets under the **subject-independent cross-validation**, with training, validation, and test splits of 80%, 10%, and 10%, respectively. We incorporate novel training strategies, including multi-sampling segmentation and index group shuffling. A gated temporal-spatial Transformer is employed to capture both temporal and spatial features. In addition, we propose a subject-level cross-entropy loss \mathcal{L}_{ce}^{sub} to enhance the learning of subject-level representations. Finally, majority voting is used for subject-level detection.

lenge for real-world clinical deployment is generalization to unseen subjects (subject-independent evaluation). Current approaches, while often strong in controlled, at-lab settings (subject-dependent), suffer a substantial performance drop when faced with this essential requirement (Wang et al., 2024b). This degradation is largely caused by inter-subject variability and shortcut learning between diagnostic labels and subject-specific characteristics. Although subjects diagnosed with AD are expected to exhibit consistent disease-related patterns, confounding factors such as age, gender, and other personal attributes may obscure these patterns. Third, existing studies are difficult to adapt to heterogeneous data. Most prior works train models on a single dataset or on datasets with identical acquisition configurations. In practice, EEG data are highly heterogeneous, not only due to demographic differences among subjects but also because of variations in recording environments, acquisition devices, channel layouts, sampling rates, and recording durations. This heterogeneity makes it challenging to transfer the detection capability of existing methods across datasets, which is critical for real-world deployment.

To address the aforementioned limitations, we propose **LEAD**, the first **Large-scale EEG** model for **AD** detection. We conduct a comprehensive review of relevant publications and public EEG repositories (by 2026), including OpenNeuro, Dryad, and Figshare, and identify 9 highly heterogeneous EEG datasets for AD and dementia detection. These datasets comprise **2,238 subjects and 427.81 hours** of recordings. To the best of our knowledge, this constitutes the world’s **largest EEG dataset** for AD detection, which is approximately **20 times larger** than those commonly used in prior publications. Building on this unique resource, we

train an EEG foundation model designed for **subject-level** Alzheimer’s detection that can handle EEG signals of **arbitrary length, channel montages, and sampling rates**. To this end, we design a gated temporal-spatial Transformer as the backbone. Using univariate patch embeddings enables the model to adapt to downstream tasks with varying input lengths and channel counts. In addition, 3D channel embeddings and sampling rate embeddings allow the model to capture spatial relationships and to distinguish samples recorded at different sampling rates. A parallel temporal-spatial attention mechanism is employed to extract both temporal and spatial features, with a learnable gated fusion module to adaptively control their relative importance. Furthermore, we introduce a subject-regularized training paradigm. A subject-level cross-entropy loss is proposed to propagate subject-level errors back to the model during training. We also design useful training techniques, such as multi-sampling segmentation and index group shuffling, to further enhance subject-level learning. Finally, we employ a domain-inspired self-supervised contrastive learning strategy for pre-training on 4 of the 9 AD datasets, along with 9 additional neurological disorder datasets, comprising a total of 4,646 subjects and 1,185.84 hours of EEG recordings. The remaining 5 AD datasets are used for fine-tuning and evaluation under a realistic yet challenging subject-independent cross-validation protocol. Figure 1 illustrates the overall pipeline of our proposed method. We compare our method against 16 baseline methods, including manual feature extraction, supervised deep learning methods, and SOTA EEG foundation models. LEAD achieves the best average ranking across all 20 evaluations on 5 datasets, far surpassing the second-best model LaBraM while using

significantly fewer pre-training resources.

The key contributions of this work are summarized as follows: 1) **The largest EEG-based AD detection dataset.** We curate the largest dataset for EEG-based AD detection to date, far surpassing prior work. 2) **First EEG Foundation Model for AD detection.** Built on this unique dataset, we develop the first foundation model for end-to-end subject-level EEG-based AD detection, adaptable to diverse recording lengths, channel topologies, and sampling rates. 3) **Superior performance.** LEAD achieves SOTA subject-level results on 5 downstream AD datasets under challenging subject-independent cross-validation.

2. Method

Problem Formulation EEG-based AD detection aims to determine whether a patient has AD. While most deep learning methods in this field focus on classifying small, individual EEG segments (sample-level classification), our approach centers on subject-level detection, which is clearly more clinically relevant. Consider an input EEG sample $\mathbf{X} \in \mathbb{R}^{C \times T}$, where C is the number of channels (electrodes) and T denotes the number of timestamps. We denote the label by y , which may correspond to different diagnostic categories, such as AD, Healthy Controls (HC), Mild Cognitive Impairment (MCI), Frontotemporal Dementia (FTD), or other types and stages of dementia. We denote the subject ID and the sampling rate by s and r , respectively. **(1) Sample-Level Classification:** The objective is to learn a model that predicts the label y for each input sample. **(2) Subject-Level Detection:** For subject-level detection, we aggregate sample-level predictions using majority voting (Sec. 2.2). The final label assigned to a subject is the class that appears most frequently among all samples associated with the same subject ID s .

2.1. Gated Temporal-Spatial Transformer

Patch Embedding. To handle EEG samples with arbitrary channel configurations and variable recording lengths, we implement a patch embedding strategy as follows. Consider an input EEG sample $\mathbf{X} \in \mathbb{R}^{C \times T}$, for a patch length L , we slice each channel into N *univariate* patches. This yields a patch tensor $\mathbf{X}_p \in \mathbb{R}^{C \times N \times L}$. Zero padding is applied when necessary to ensure that T is divisible by L , resulting in $N = \lceil T/L \rceil$. Each patch is then projected into a D -dimensional embedding space through a linear mapping $\mathbf{W} \in \mathbb{R}^{L \times D}$, producing patch embeddings $\mathbf{E} \in \mathbb{R}^{C \times N \times D}$. A fixed temporal positional embedding $\mathbf{PE} \in \mathbb{R}^{N \times D}$ is added and broadcast across all C channels. The final patch embeddings are obtained as:

$$\mathbf{E} \leftarrow \mathbf{X}_p \mathbf{W} + \text{Broadcast}(\mathbf{PE}), \quad \mathbf{E} \in \mathbb{R}^{C \times N \times D} \quad (1)$$

3D Channel Embedding. To enable the model flexibly adapt to arbitrary channel configurations and to learn spatial relationships among channels, we employ the 3D EEG channel embedding introduced in NeurIPT (Fang et al., 2025), with minor modifications. Let $\mathbf{P} \in \mathbb{R}^{C \times 3}$ denote the 3D channel coordinate matrix, where the c -th channel has spatial coordinates $\mathbf{P}_c = (x_c, y_c, z_c)$ for $c = 1, \dots, C$. The \mathbf{P}_c denotes the relative positions of EEG channels following the international 10-20 system (Homan et al., 1987). To encode spatial information in a parameter-free manner, we apply sinusoidal positional encoding independently along each spatial axis and concatenate the resulting embeddings to form a D -dimensional channel embedding. Given the target embedding dimension D , we automatically allocate dimensions across the three spatial axes as:

$$D_x = \left\lfloor \frac{D}{3} \right\rfloor, \quad D_y = \left\lfloor \frac{D}{3} \right\rfloor, \quad D_z = D - D_x - D_y \quad (2)$$

For an axis coordinate $p \in \{x_c, y_c, z_c\}$, we define an axis-specific sinusoidal embedding $\text{CE}(p) \in \mathbb{R}^{D_p}$, where $D_p \in \{D_x, D_y, D_z\}$, as:

$$\begin{aligned} \text{CE}(p)_{2i} &= \sin\left(p \cdot 10000^{-\frac{2i}{D_p}}\right), \\ \text{CE}(p)_{2i+1} &= \cos\left(p \cdot 10000^{-\frac{2i}{D_p}}\right) \end{aligned} \quad (3)$$

where $i = 0, 1, \dots, \left\lfloor \frac{D_p}{2} \right\rfloor - 1$. We compute axis-wise embeddings for each channel and concatenate them to obtain the final 3D channel embedding:

$$\mathbf{e}_c = [\text{CE}(x_c) \parallel \text{CE}(y_c) \parallel \text{CE}(z_c)] \in \mathbb{R}^D, \quad c = 1, \dots, C \quad (4)$$

which yields the channel embedding matrix $\mathbf{CE} \in \mathbb{R}^{C \times D}$ by stacking $\{\mathbf{e}_c\}_{c=1}^C$. The channel embeddings are then broadcast and added to all N patch embeddings:

$$\mathbf{E} \leftarrow \mathbf{E} + \text{Broadcast}(\mathbf{CE}), \quad \mathbf{E} \in \mathbb{R}^{C \times N \times D} \quad (5)$$

In practice, 3D coordinate information can be readily obtained given the electrode montage and channel names using the MNE Python package (Gramfort et al., 2013).

Sampling Rate Embedding. Since the sampling rate critically affects the temporal patterns of EEG signals, even for recordings of identical duration, we design a sampling rate embedding module to explicitly inform the model of the temporal scale of the input. Given each EEG sample is associated with a sampling rate label r , we introduce a learnable embedding lookup table that maps each sampling-rate marker r to a D -dimensional embedding vector $\mathbf{e}_r \in \mathbb{R}^D$. The sampling rate embedding is broadcast and added to all $C \times N$ patch embeddings:

$$\mathbf{E} \leftarrow \mathbf{E} + \text{Broadcast}(\mathbf{e}_r), \quad \mathbf{E} \in \mathbb{R}^{C \times N \times D} \quad (6)$$

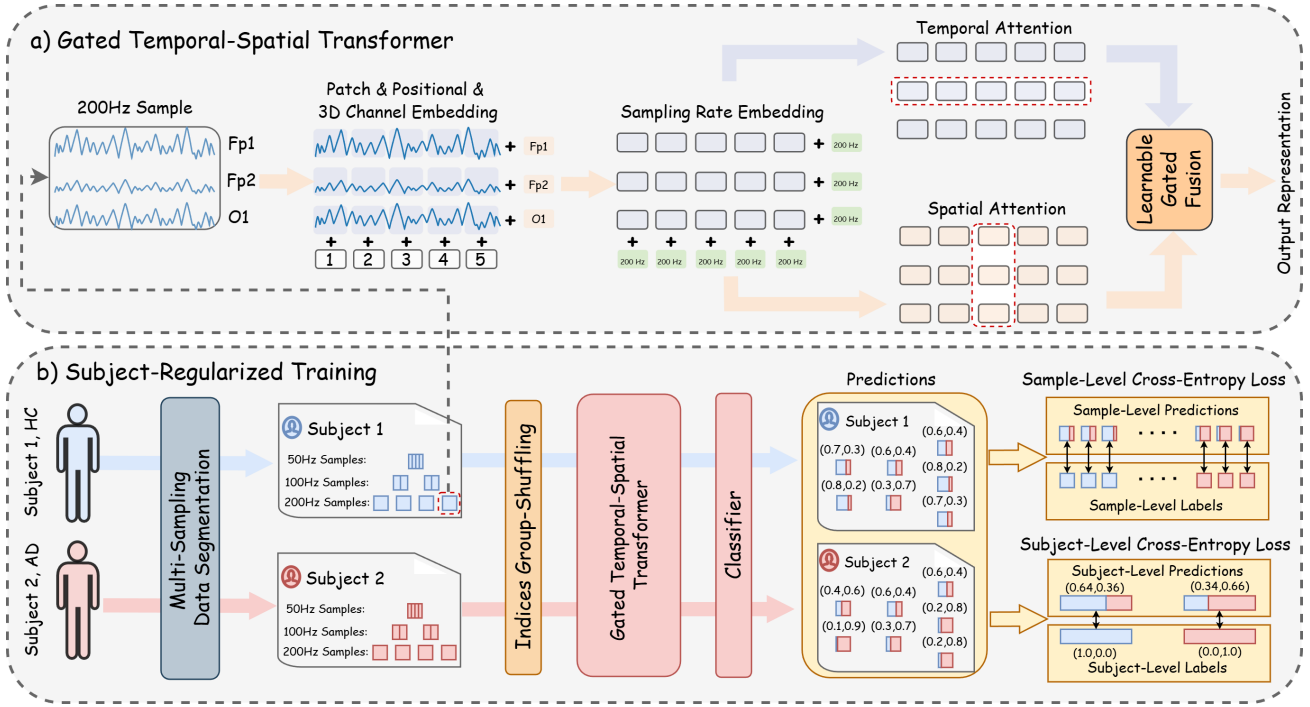


Figure 2. a) Gated Temporal Spatial Transformer. Input EEG samples are first sliced into univariate patches. These patches are mapped to patch embeddings, to which temporal positional embeddings, 3D channel embeddings, and sampling rate embeddings are added to form the final patch representations. A parallel temporal-spatial attention mechanism is then applied along both the temporal and channel dimensions. The resulting features from the two dimensions are combined using a learnable gated fusion module. **b) Subject-Regularized Training.** Each subject’s EEG recordings are segmented into windows with varying sampling rates, such as 200 Hz, 100 Hz, and 50 Hz, using a multi-sampling segmentation strategy. Index group shuffling ensures that each training batch contains sufficient samples from the same subject, which facilitates subject-level learning. The classifier produces sample-level predictions that are aggregated into subject-level predictions. Both two-level predictions are used to compute cross-entropy losses.

This embedding strategy enables the model to flexibly adapt to arbitrary sampling rates in downstream tasks. In addition, a multi-sampling segmentation scheme is jointly employed during data preprocessing (see Appendix F.2), which facilitates multi-scale representation learning and effectively increases the number of training samples.

Parallel Temporal-Spatial Attention. Given the input representation $\mathbf{E} \in \mathbb{R}^{C \times N \times D}$, where C denotes the number of channels, N the number of temporal patch embeddings per channel, and D the embedding dimension, we apply temporal and spatial self-attention in parallel to jointly model temporal dynamics and spatial dependencies. **(1) Temporal Attention.** Self-attention is applied independently within each channel along the temporal dimension:

$$\mathbf{E}_c^T = \text{Attn}(\mathbf{E}_c, \mathbf{E}_c, \mathbf{E}_c) \in \mathbb{R}^{N \times D}, \quad c = 1, \dots, C, \quad (7)$$

where $\mathbf{E}_c \in \mathbb{R}^{N \times D}$ denotes the sequence of patch embeddings for the c -th channel. We stack the output of all channels yields $\mathbf{E}^T \in \mathbb{R}^{C \times N \times D}$. **(2) Spatial Attention.** Spatial self-attention is applied independently across channels at each temporal patch index:

$$\mathbf{E}_n^S = \text{Attn}(\mathbf{E}_n, \mathbf{E}_n, \mathbf{E}_n) \in \mathbb{R}^{C \times D}, \quad n = 1, \dots, N, \quad (8)$$

where $\mathbf{E}_n \in \mathbb{R}^{C \times D}$ denotes the set of channel embeddings at the n -th temporal patch. We stack the output of all channels yields $\mathbf{E}^S \in \mathbb{R}^{C \times N \times D}$. **(3) Gated Fusion.** The temporal and spatial attention outputs are fused through a learnable gated module. Specifically, a feature-wise gate is computed as:

$$\mathbf{G} = \sigma([\mathbf{E}^T \parallel \mathbf{E}^S] \mathbf{W}_f), \quad \mathbf{G} \in \mathbb{R}^{C \times N \times D}, \quad (9)$$

where $\sigma(\cdot)$ denotes the sigmoid function, \parallel denotes concatenation, and $\mathbf{W}_f \in \mathbb{R}^{2D \times D}$. The final output representation is obtained via element-wise gated fusion:

$$\mathbf{E} = \mathbf{G} \odot \mathbf{E}^T + (1 - \mathbf{G}) \odot \mathbf{E}^S, \quad \mathbf{E} \in \mathbb{R}^{C \times N \times D} \quad (10)$$

where \odot denotes element-wise multiplication. The learnable gated fusion allows the model to automatically learn the relative importance of temporal and spatial features.

Classifier. After M stacked blocks comprising attention modules, layer normalization, and feedforward networks, the model outputs a representation $\mathbf{E} \in \mathbb{R}^{C \times N \times D}$. The final representation $\mathbf{E}_f \in \mathbb{R}^{C \times D}$ is obtained by selecting the last patch embedding for each channel. The resulting representation \mathbf{E}_f is then fed into an MLP classifier $c(\cdot)$ to produce a sample-level prediction \hat{y} , which is used to compute the sample-level cross-entropy loss \mathcal{L}_{ce}^{sam} .

2.2. Subject-Regularized Training

Subject-Level Cross-Entropy Loss. Previous studies have shown that high sample-level prediction accuracy does not necessarily result in high subject-level detection performance (Wang et al., 2024c), which may stem from imbalances in the number of samples per subject and inherent subject-specific variability. To address this issue, we introduce a subject-level cross-entropy loss \mathcal{L}_{ce}^{sub} to explicitly enforce predictive consistency across samples from the same subject. We present the pseudocode in Algorithm 1. For each unique subject s present in a training batch, we compute a subject-level prediction by averaging the model’s outputs over all samples associated with that subject. The loss \mathcal{L}_{ce}^{sub} is then computed as the cross-entropy between these aggregated predictions and the subject’s ground-truth label (the label of any sample in that subject) Appendix B).

Algorithm 1 Subject-level Cross-Entropy Loss

```

1: Input: Predictions  $\hat{\mathbf{y}} \in \mathbb{R}^B$ , labels  $\mathbf{y} \in \mathbb{R}^B$ , subject
   IDs  $\mathbf{s} \in \mathbb{R}^B$ .  $B$  is the size of the current batch.
2: Output: Subject-level loss  $\mathcal{L}_{ce}^{sub}$ 
3:  $\mathcal{U} \leftarrow \text{Unique}(\mathbf{s})$  # set of subject IDs in the batch
4:  $\mathcal{Z} \leftarrow []$ ,  $\mathcal{Y} \leftarrow []$  # lists for mean predictions/labels
5: for each  $u \in \mathcal{U}$  do
6:    $\mathcal{M} \leftarrow \{i \mid \mathbf{s}_i = u\}$  # indices of subject  $u$ 
7:    $\bar{\mathbf{z}} \leftarrow \frac{1}{|\mathcal{M}|} \sum_{i \in \mathcal{M}} \hat{\mathbf{y}}_i$  # subject  $u$  mean prediction
8:   Choose any  $i^* \in \mathcal{M}$ , set  $\mathbf{y}_u \leftarrow \mathbf{y}_{i^*}$  # subject  $u$  true
   label
9:   Append  $\bar{\mathbf{z}}$  to  $\mathcal{Z}$  and  $\mathbf{y}_u$  to  $\mathcal{Y}$ 
10: end for
11:  $\mathcal{L}_{ce}^{sub} \leftarrow \text{CrossEntropy}(\mathcal{Z}, \mathcal{Y})$ 
12: return  $\mathcal{L}_{ce}^{sub}$ 
    
```

Index Group-Shuffling. In practical training with a large number of subjects, the probability that multiple samples from the same subject appear within the batch decreases, reducing the effectiveness of subject-level learning. To mitigate this issue, we introduce a new index-group-shuffling algorithm that dynamically reorders indices for each epoch. The pseudocode is provided in Algorithm 2. The computational cost of this algorithm is negligible, as it requires only sorting and shuffling. The algorithm ensures that, for every subject included in a batch, at least a predefined group size of samples from that subject is present, while maintaining enough randomness.

Overall Loss Function. The final cross-entropy loss for supervised learning or fine-tuning is $\mathcal{L}_{ce} = \alpha \mathcal{L}_{ce}^{sam} + \beta \mathcal{L}_{ce}^{sub}$, where $\alpha, \beta \in [0, 1]$ control the weight of sample-level and subject-level cross-entropy losses.

Majority Voting. Since our model is trained and makes initial predictions on segmented, fixed-length EEG samples, a post-processing step is typically required during testing

to convert sample-level classifications into final subject-level detections. A commonly used method is the majority vote mechanism (Ieracitano et al., 2019a). Specifically, the subject-level label is derived by taking the mode (the majority label) of all sample-level predictions for that subject.

Algorithm 2 Index Group-Shuffling

```

1: Input: Subject IDs  $\mathbf{s} \in \mathbb{R}^N$ , group size  $G$ , batch size
    $B$ .  $N$  is the total number of samples in the training set.
2: Output: A shuffled index permutation  $\pi \in \{1, \dots, N\}^N$ 
   of all training samples.
3:  $\mathbf{p} \leftarrow \text{argsort}(\mathbf{s})$  # sort indices by subject IDs
4:  $\mathcal{G} \leftarrow []$  # list of groups
5: for  $i = 1$  to  $N$  step  $G$  do
6:    $\mathcal{G} \leftarrow \mathcal{G} \cup \{\mathbf{p}[i : \min(i + G - 1, N)]\}$  # groups
7: end for
8:  $\text{Shuffle}(\mathcal{G})$  # shuffle group order
9:  $\mathbf{q} \leftarrow \text{Concat}(\mathcal{G})$  # flatten groups
10:  $\mathcal{B} \leftarrow []$  # list of batches
11: for  $j = 1$  to  $N$  step  $B$  do
12:    $\mathbf{u} \leftarrow \mathbf{q}[j : \min(j + B - 1, N)]$  # form a batch
13:    $\text{Shuffle}(\mathbf{u})$  # shuffle within batch
14:    $\mathcal{B} \leftarrow \mathcal{B} \cup \{\mathbf{u}\}$ 
15: end for
16:  $\pi \leftarrow \text{Concat}(\mathcal{B})$  # flatten batches back
17: return  $\pi$ 
    
```

2.3. Domain-Inspired Self-Supervised Pre-training

We employ both sample-level and subject-level medical contrastive learning for self-supervised pre-training (Wang et al., 2023). Sample-level contrastive learning performs instance discrimination, treating different augmented views of the same sample as positive pairs and views from other samples as negative pairs. The augmentation methods are described in Appendix D. The subject-level contrastive learning leverages subject IDs as guidance: samples from the same subject are treated as positive pairs, while those from different subjects are treated as negative pairs. Compared with masked autoencoding (He et al., 2022), subject-level contrastive learning is more suitable for our goal of **capturing subject-level representations** for AD detection, under the assumption that all samples from a subject collected in a short period share the same label (See preliminaries in Appendix B). We also incorporate the index group-shuffling algorithm (Alg. 2) to maintain the probability that samples with the same subject ID co-occur within a mini-batch. The overall self-supervised pre-training objective is a weighted sum of the two contrastive losses: $\mathcal{L}_{co} = \lambda_1 \mathcal{L}_{co}^{sam} + \lambda_2 \mathcal{L}_{co}^{sub}$, where $\lambda_1 + \lambda_2 = 1$, and $\lambda_1, \lambda_2 \in [0, 1]$ control the relative importance. More details are provided in Appendix C.

3. Experiments

3.1. Setup

Datasets. We categorize EEG datasets utilized in this paper into two groups: those containing data from subjects with Alzheimer’s Disease (AD datasets) and those without (Non-AD datasets). We conducted a comprehensive review of relevant publications and public EEG repositories (e.g., OpenNeuro, Dryad, figshare) published before 2026. This effort identified 8 public AD datasets. In total, we utilize 8 public and 1 private AD datasets, most of which consist of resting-state recordings: **AD-Auditory** (Lahijanian et al., 2024), **BrainLat** (Prado et al., 2023), **P-ADIC** (Shor et al., 2021), **CAUEEG** (Kim et al., 2023), **ADFSU** (Vicchiotti et al., 2023), **ADFTD** (Miltiadous et al., 2023b), **ADSZ** (Alves et al., 2022), **APAVA** (Escudero et al., 2006), and **CNBPM** (Amezquita-Sanchez et al., 2019). Together, these datasets comprise **2,238 subjects and 427.81 hours** of recordings, forming the **world’s largest EEG-AD corpus** reported so far. We also include 9 non-AD domain-relevant resting-state datasets that include recordings from both healthy subjects and patients with other neurological conditions (e.g., Parkinson’s disease, depression, ADHD). These datasets are: **BACA-RS** (Getzmann et al., 2024), **Depression** (Cavanagh et al., 2019), **FEPCR** (Phalen et al., 2020), **MCEF-RS** (Chenot et al., 2024), **PD-RS** (Singh et al., 2023), **PEARL-Neuro** (Dzianok & Kublik, 2024), **SRM-RS** (Hatlestad-Hall et al., 2022), **TDBrain** (Van Dijk et al., 2022), **TUEP** (Veloso et al., 2017), account for total **2848 subjects, 805.62 hours**. Details in the Appendix F.1.

Data Preprocessing. The preprocessing pipeline is presented in Appendix F.2, and the statistics of the processed datasets are summarized in Table 6. A more detailed per-dataset preprocessing description is available in Appendix F.3. For pre-training, we leverage all 9 Non-AD datasets together with 4 AD datasets, resulting in a total of **4,646 subjects, 1,185.84 hours, and 7,431,484 samples** (representing 2s, 4s, and 8s segments at 200Hz, 100Hz, and 50Hz sampling rates). The remaining 5 AD datasets are reserved for downstream evaluation, resulting in a total of **440 subjects, 47.59 hours, and 303,570 samples**.

Baselines. We compare our method against **16** baselines, including 1 manual feature-extraction approach, 11 supervised deep-learning models, and 4 large EEG foundation models. These selected baselines are state-of-the-art methods or have shown strong performance in EEG classification tasks. The feature-based method extracts **Statistical, Spectral, Power, and Complexity** features (see Appendix E) commonly used for EEG-based AD detection, followed by classification with a linear classifier. The 11 supervised learning methods include **EEGConformer** (Song et al., 2022), **EEGInception** (Zhang et al., 2021), **EEGNet** (Lawhern et al., 2018), **iTransformer** (Liu et al., 2023b), **MedGNN** (Fan et al.,

2025), **Medformer** (Wang et al., 2024b), **MNet** (Watanabe et al., 2024), **ModernTCN** (Luo & Wang, 2024), **PatchTST** (Nie, 2023), **TCN** (Bai et al., 2018), **TimesNet** (Wu et al., 2023). The 4 EEG foundation models are **BIOT** (Yang et al., 2024), **LaBraM** (Jiang et al., 2024b), **CBraMod** (Wang et al., 2025), **CSBrain** (Zhou et al., 2025).

Training & Parameter Settings. Self-supervised pre-training is conducted for 30 epochs without early stopping, followed by fine-tuning for up to 200 epochs with early stopping (patience=15) based on the best sample-level F1. Batch sizes are 2048 for pre-training and 512 for supervised learning. We use AdamW with learning rates of 2×10^{-4} (pre-training) and 1×10^{-4} (fine-tuning), scheduled by CosineAnnealingLR. We employ 14 evaluation metrics, including sample-level accuracy, precision (macro-averaged), sensitivity (macro-averaged), specificity (macro-averaged), F1 score (macro-averaged), AUROC (macro-averaged), and AUPRC (macro-averaged), and their corresponding subject-level metrics computed via majority voting (Para. 2.2). The contrastive loss coefficients in self-supervised pre-training are set to $\lambda_1 = 0.25$ and $\lambda_2 = 0.75$. Both sample-level and subject-level cross-entropy losses are set to $\alpha = \beta = 0.5$ in the fine-tuning stage. The *group_size* for index group shuffling is set to 32 and 8 for the pre-training and fine-tuning stages, respectively. For self-supervised pre-training, all subjects from the pre-training datasets are used. For supervised learning and fine-tuning, we adopt Monte Carlo cross-validation (Xu & Liang, 2001) with a subject-independent (Wang et al., 2024b) 8:1:1 train/validation/test split, ensuring no subject overlap while preserving randomness across seeds. To enable cross-domain transfer, no pre-training subjects or datasets are used in fine-tuning. For 4 foundation model baselines, we fine-tune their released checkpoints. Each evaluation is repeated with five random seeds (41-45), reporting the mean and standard deviation. Experiments are run on 8 NVIDIA RTX A6000 GPUs with Python 3.10 and PyTorch 2.5.1+cu121. Further details for each method are provided in Appendix E.

3.2. Results

Performance Comparison with Baselines. We compare LEAD with 16 baseline methods on 5 downstream datasets. The F1 score and AUROC results are reported in Table 2, while the complete results for all 7 evaluation metrics are provided in Appendix G.1. Our method achieves top-1 performance in 18 out of 20 evaluations. Notably, LEAD consistently outperforms all competing approaches across subject-level F1 score and AUROC, demonstrating strong potential for real-world clinical detection. Furthermore, our method surpasses existing EEG foundation models despite being pre-trained on only 1,185.84 hours of EEG data, which is substantially less than the approximately 2,000 hours used by LaBraM and more than 9,000 hours used by

An EEG Foundation Model for Alzheimer’s Disease Detection

Table 2. Method Comparison Results on 5 Datasets. F1 score and AUROC comparison results of 16 baselines and our method. The full table of all 7 metrics is available in Appendix G.1. The **Top-1**, **Top-2**, and **Top-3** results are highlighted in red, blue, and green.

Datasets	ADFSU (4,048 Samples) (92 Subjects) (HC vs AD)		ADFTD (167,083 Samples) (88 Subjects) (HC vs AD vs FTD)		ADSZ (1,128 Samples) (48 Subjects) (HC vs AD)		APAVA (9,282 Samples) (23 Subjects) (HC vs AD)		CNBPM (122,029 Samples) (189 Subjects) (HC vs MCI vs AD)		
	Methods	F1 Score	AUROC	F1 Score	AUROC	F1 Score	AUROC	F1 Score	AUROC	F1 Score	AUROC
Sample-Level Classification											
ManualFeature	75.67±11.41	80.90±8.87	44.73±3.88	62.89±4.31	58.42±21.26	67.20±15.34	63.22±6.51	66.49±5.78	43.00±6.36	61.29±6.44	
EEGConformer	94.22±3.28	98.87±0.95	58.59±3.84	80.61±3.90	94.73±3.47	98.50±1.48	73.05±4.93	83.07±3.70	59.17±8.85	81.76±8.20	
EEGInception	90.88±2.13	98.73±0.75	62.69±4.06	84.01±2.76	92.60±4.44	98.06±1.66	67.84±4.60	78.04±4.19	58.56±8.02	81.73±8.18	
EEGNet	74.48±9.91	85.88±7.95	40.31±6.74	60.93±4.42	64.90±12.88	77.18±19.10	67.84±4.60	78.04±4.19	38.57±6.52	63.51±7.95	
iTransformer	76.80±2.31	88.16±1.86	54.33±3.67	73.98±4.02	73.13±4.75	81.86±4.90	72.13±2.30	85.53±1.00	51.37±8.01	74.99±10.16	
MedGNN	90.09±2.37	98.06±1.42	67.67±4.60	85.52±2.57	88.59±8.01	95.90±4.10	67.54±7.95	81.39±3.83	58.68±7.50	82.13±7.35	
Medformer	87.15±1.91	97.48±1.32	64.83±6.72	84.13±3.27	88.73±5.76	94.18±3.72	67.42±2.44	78.38±2.75	60.39±7.68	82.17±7.87	
MNet	76.19±2.82	92.75±5.08	59.91±9.77	82.30±5.04	79.21±7.35	88.87±5.92	52.98±8.72	79.85±3.17	47.04±9.76	77.03±11.79	
ModernTCN	75.09±3.18	91.94±1.84	58.52±3.71	77.25±3.33	75.73±4.05	84.42±4.30	58.42±0.76	75.88±2.41	55.94±8.10	77.85±9.30	
PatchTST	76.03±4.27	89.12±1.95	50.95±4.04	71.30±4.75	71.05±10.02	79.10±12.54	52.39±2.65	73.76±3.11	49.78±6.10	71.52±9.58	
TCN	90.10±13.13	98.82±0.73	64.26±2.40	82.94±1.89	88.93±9.23	94.02±6.85	74.81±4.47	85.84±3.92	58.71±5.02	82.01±6.02	
TimesNet	82.08±6.29	95.21±2.45	58.66±5.68	79.18±3.39	83.80±3.60	88.12±9.12	55.95±6.89	56.01±4.93	56.19±6.63	79.18±7.74	
BIOT	88.94±2.69	96.78±3.04	69.79±5.90	86.85±4.77	90.83±4.72	96.73±2.98	79.55±5.36	92.92±2.77	54.79±9.52	77.95±11.46	
LaBraM	92.24±3.38	98.90±0.53	75.64±4.68	91.22±2.72	91.12±4.50	97.54±1.88	71.65±3.35	85.61±1.20	52.66±7.11	78.44±9.59	
CBraMod	92.32±4.27	98.47±1.49	68.33±4.53	86.95±2.89	83.70±9.28	96.67±3.69	74.10±2.40	83.10±1.85	53.93±6.87	78.68±9.10	
CSBrain	91.11±2.34	98.23±0.51	69.39±2.63	86.82±1.28	93.16±4.03	98.87±1.14	61.69±8.63	68.20±1.53	60.30±5.41	83.39±5.73	
LEAD	97.06±1.02	99.92±0.07	81.01±5.02	94.03±1.33	97.42±2.74	100.00±0.00	83.70±5.30	92.51±4.33	60.20±6.83	79.10±10.21	
Subject-Level Detection											
ManualFeature	81.05±20.29	80.00±18.71	54.26±7.80	69.80±2.94	63.05±30.68	70.00±24.49	57.33±19.60	65.00±12.25	43.95±7.64	61.43±4.16	
EEGConformer	100.00±0.00	100.00±0.00	68.45±15.21	79.13±8.16	100.00±0.00	100.00±0.00	65.33±16.00	70.00±10.00	58.42±8.60	70.00±5.80	
EEGInception	100.00±0.00	100.00±0.00	79.47±17.70	86.23±10.23	100.00±0.00	100.00±0.00	70.67±21.33	75.00±15.81	59.77±8.06	70.71±5.71	
EEGNet	78.37±21.07	81.25±18.54	54.82±14.34	70.60±8.38	61.38±22.11	66.67±18.26	70.67±21.33	75.00±15.81	34.02±11.43	55.00±7.35	
iTransformer	66.01±17.61	65.00±12.25	67.17±9.15	78.21±5.36	100.00±0.00	100.00±0.00	84.00±13.06	85.00±12.25	52.85±8.58	67.14±5.25	
MedGNN	100.00±0.00	100.00±0.00	75.23±4.81	83.41±3.30	96.57±6.86	96.67±6.67	65.33±16.00	70.00±10.00	52.18±11.32	65.71±7.69	
Medformer	100.00±0.00	100.00±0.00	78.98±12.08	84.84±8.41	100.00±0.00	100.00±0.00	73.33±0.00	75.00±0.00	60.93±6.49	72.14±4.16	
MNet	58.82±17.61	60.00±12.25	68.63±17.53	80.08±9.49	89.90±13.38	90.00±13.33	41.33±16.00	55.00±10.00	39.97±4.38	62.14±4.29	
ModernTCN	58.82±17.61	60.00±12.25	74.39±11.35	82.82±6.50	89.71±8.40	90.00±8.16	33.33±0.00	50.00±0.00	61.96±9.90	72.86±5.35	
PatchTST	77.12±18.02	75.00±15.81	65.04±14.32	77.26±7.62	86.29±19.99	86.67±19.44	33.33±0.00	50.00±0.00	51.35±9.07	67.14±4.16	
TCN	96.08±7.84	95.00±10.00	82.80±6.10	87.38±4.32	96.57±6.86	96.67±6.67	73.33±0.00	75.00±0.00	62.66±3.41	72.86±2.86	
TimesNet	84.97±21.64	85.00±20.00	64.23±17.73	78.57±9.45	96.57±6.86	96.67±6.67	33.33±0.00	50.00±0.00	55.52±4.93	67.86±3.91	
BIOT	100.00±0.00	100.00±0.00	88.10±9.72	90.71±7.61	90.83±4.72	96.73±2.98	95.00±10.00	94.67±10.67	55.74±8.58	67.86±5.98	
LaBraM	100.00±0.00	100.00±0.00	91.14±8.64	93.77±6.16	100.00±0.00	100.00±0.00	70.67±21.33	75.00±15.81	50.11±6.53	65.00±3.50	
CBraMod	100.00±0.00	100.00±0.00	82.21±6.30	87.10±3.77	89.07±14.85	90.00±13.33	73.33±0.00	75.00±0.00	50.60±10.89	65.71±7.00	
CSBrain	100.00±0.00	100.00±0.00	78.33±7.52	84.56±4.61	100.00±0.00	100.00±0.00	57.33±19.60	65.00±12.25	62.41±5.80	72.86±3.64	
LEAD	100.00±0.00	100.00±0.00	93.95±4.95	95.36±3.85	100.00±0.00	100.00±0.00	100.00±0.00	100.00±0.00	65.94±6.66	75.00±5.05	

Table 3. EEG Paradigms Comparison. Each ADFTD subject was recorded under two paradigms: resting-state eyes-closed and photic-stimulation eyes-open, with varying recording lengths. We evaluate model performance on each paradigm separately and both.

Datasets	Paradigms	Accuracy	Precision	Sensitivity	Specificity	F1 Score	AUROC	AUPRC
ADFTD (Sample-Level) (HC vs AD vs FTD)	Resting-State (19.40h)	55.90±4.43	53.22±6.63	52.29±5.21	76.91±2.39	50.67±5.83	74.02±6.19	59.78±8.63
	Photic-Stimulation (7.25h)	58.23±9.57	58.13±12.16	56.24±10.83	78.83±4.93	55.60±11.70	72.08±11.15	60.17±13.52
	Both (26.64h)	81.70±4.74	82.93±4.40	80.78±4.95	90.52±2.45	81.01±5.02	94.03±1.33	90.37±2.14
ADFTD (Subject-Level) (HC vs AD vs FTD)	Resting-State (19.40h)	64.00±10.20	56.14±20.90	61.11±11.52	80.95±5.48	55.49±15.08	71.03±8.48	54.29±10.49
	Photic-Stimulation (7.25h)	60.00±10.95	61.67±18.05	60.56±11.84	79.68±5.80	58.58±14.37	70.12±8.80	54.32±9.98
	Both (26.64h)	94.00±4.90	95.67±3.59	93.89±5.09	96.83±2.61	93.95±4.95	95.36±3.85	91.56±6.91

Table 4. Per-Subject Analysis. We report per-subject results on the ADFTD dataset under the leave-one-subject-out setting and analyze the factors influencing model performance, including demographic characteristics, recording length, MMSE score, and dementia category.

Label	Gender		Age		Length		MMSE			Dementia Class		
	M	F	<65	≥65	<0.32h	≥0.32h	0-17	18-24	25-30	AD	HC	FTD
Subject Number	44	44	38	50	45	43	13	42	33	36	29	23
Sample-level Accuracy	78.51%	80.98%	79.14%	80.20%	75.96%	83.70%	81.42%	79.49%	79.40%	82.28%	84.77%	69.43%
Subject-level Accuracy	95.45%	90.91%	97.37%	90.00%	88.89%	97.67%	100.00%	90.48%	93.94%	94.44%	100.00%	82.61%

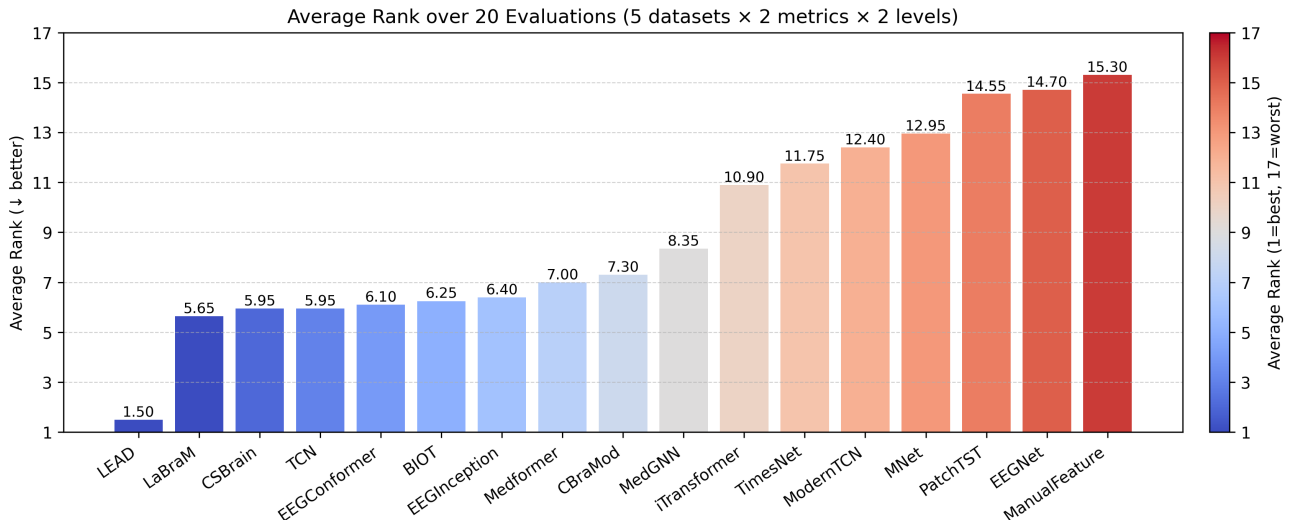


Figure 3. a) Average performance rank of 17 methods across all 5 datasets \times 2 evaluation metrics \times 2 levels. For example, the value 1.5 of LEAD indicates an average rank of 1.5 over the total 20 evaluations. **Lower ranks and a deeper blue indicate better performance.**

CBraMod and CSBrain. These results highlight the effectiveness of the proposed backbone, subject-level training strategy, and domain-inspired pre-training paradigm, as well as the careful selection of pre-training data.

EEG Paradigms Comparison. We evaluate the ADFTD dataset across three paradigms: resting-state, photic-stimulation, and both. Results are shown in Table 3. Using both paradigms substantially outperforms the individual paradigms, achieving a subject-level F1 of 93.95% versus 55.58% (resting-state) and 58.58% (photic-stimulation). While it remains unclear whether this gain arises from longer EEG recording time or complementary paradigm features, the evidence of performance indicates that **using both of these two paradigms is non-detrimental and strongly likely to be beneficial for EEG-based AD detection.**

Per-Subject Analysis. We further explore per-subject performance across demographics, recording length, MMSE score, and clinical subgroups under the leave-one-subject-out (LOSO) setting on ADFTD. The full results of each subject are in Appendix G.2. A comparison among factors is in Table 4. Longer recordings (≥ 0.32 h) consistently yield higher accuracy at both the sample and subject levels, highlighting the importance of sufficient EEG recording length. Subjects younger than 65 years show higher subject-level accuracy than older subjects, suggesting increased variability in elderly EEG recordings. Performance also varies with cognitive status: subjects with lower MMSE scores (0-17) are classified most reliably, whereas intermediate MMSE ranges (18-24) exhibit reduced accuracy. In terms of dementia category, the model achieves perfect subject-level accuracy in healthy controls, strong performance in AD, and noticeably lower accuracy in FTD, indicating that FTD remains the most challenging to distinguish.

Ablation Study. We conduct an ablation study on the ADFTD dataset to evaluate the contribution of each module in our proposed method. The results are reported in Table 5. Overall, removing any individual component results in a degradation of more than 1% in the F1 score at both the sample- and subject-levels, indicating that all modules contribute positively to the final performance. The most significant performance drops are observed when pre-training is removed and when the sampling rate embedding is excluded. Specifically, disabling pre-training or sampling-rate embedding results in approximately a 5% decrease in sample-level F1 score and an 8% decrease in subject-level F1 score. The degradation caused by removing contrastive pre-training highlights the importance of the proposed domain-inspired pre-training strategy. In addition, the performance drop observed when removing the sampling rate embedding and the multi-sampling segmentation strategy indicates that using sampling rate embedding with a single sampling rate leads to only a minor performance loss, whereas training on multi-sampling data without sampling rate embedding causes a substantial degradation. This suggests that the model struggles to distinguish samples with different sampling rates when no explicit sampling rate information is provided. Other components, including index group shuffling and the subject-level cross-entropy loss, also consistently improve performance at both the sample and subject levels. Overall, the ablation results demonstrate the effectiveness of the proposed design choices and confirm that our method does not contain redundant modules.

4. Conclusion and Limitations

Conclusion. This paper introduces LEAD, the first foundation model for EEG-based Alzheimer’s disease detec-

Table 5. Ablation Study. We investigate the effectiveness of individual modules and design choices in our method through systematic ablation, in which each component is removed separately.

Datasets	Paradigms	Accuracy	Precision	Sensitivity	Specificity	F1 Score	AUROC	AUPRC
ADFTD (Sample-Level) (167,083 Samples) (HC vs AD vs FTD)	No Pre-training	76.02±4.61	76.96±3.96	74.58±4.96	87.61±2.46	74.63±4.96	90.16±2.68	83.80±3.60
	No Index Group Shuffling	80.49±4.87	81.33±4.65	79.65±5.06	89.95±2.51	79.73±5.11	93.51±1.65	89.48±2.46
	No Subject Cross-Entropy Loss	80.59±4.87	81.61±4.38	79.76±5.21	89.97±2.55	79.92±5.18	93.59±1.57	89.61±2.51
	No Sampling Rate Embedding	76.73±4.51	78.37±4.53	75.46±4.35	87.93±2.24	75.84±4.49	90.96±1.76	85.66±2.69
	No Multi-Sampling Segmentation	80.54±5.08	81.21±4.69	79.78±5.43	89.98±2.67	79.87±5.34	93.32±1.84	89.24±2.84
	LEAD (Full)	81.70±4.74	82.93±4.40	80.78±4.95	90.52±2.45	81.01±5.02	94.03±1.33	90.37±2.14
ADFTD (Subject-Level) (88 Subjects) (HC vs AD vs FTD)	No Pre-training	86.00±8.00	89.22±6.97	85.56±8.13	92.54±4.22	85.42±8.45	89.05±6.17	81.02±10.64
	No Index Group Shuffling	92.00±4.00	94.00±3.09	92.22±4.08	95.87±2.09	92.04±4.00	94.05±3.08	88.89±5.58
	No Subject Cross-Entropy Loss	92.00±4.00	94.00±3.09	92.22±4.08	95.87±2.09	92.04±4.00	94.05±3.08	88.89±5.58
	No Sampling Rate Embedding	86.00±8.00	88.44±7.18	85.56±8.13	92.70±4.09	85.06±8.85	89.13±6.10	80.24±11.29
	No Multi-Sampling Segmentation	92.00±4.00	94.00±3.09	92.22±4.08	95.87±2.09	92.04±4.00	94.05±3.08	88.89±5.58
	LEAD (Full)	94.00±4.90	95.67±3.59	93.89±5.09	96.83±2.61	93.95±4.95	95.36±3.85	91.56±6.91

tion, trained on the world’s largest EEG AD corpus. We design a gated temporal-spatial Transformer that adapts to EEG recordings of arbitrary length, channel configuration, and sampling rate. We further propose a subject-regularized training strategy, including subject-level cross-entropy, index-group shuffling, and multi-sampling segmentation, to enhance subject-level feature learning. Medical contrastive pre-training is conducted on 13 datasets, including 4 AD datasets and 9 non-AD neurological disorder datasets. Extensive experiments on 5 AD downstream datasets demonstrate that LEAD achieves the best overall ranking compared with 16 baseline methods across 20 evaluations. These results validate the effectiveness of the proposed architectural and training designs and highlight the significant benefits of large-scale EEG pre-training for EEG-based AD detection.

Limitation. Although performance on classifying AD vs HC and AD vs other dementias, such as FTD, is relatively strong, typically achieving a subject-level F1 score of more than 95%, performance on dementia-stage classification that separates AD, MCI, and HC remains limited, with a subject-level F1 score of approximately 66%. This highlights the continued challenge of AD stage detection. A likely explanation lies in the overlapping distribution of dementia stage categories. AD is a progressive neurodegenerative disease: healthy older adults may transition into MCI, and some MCI cases eventually progress to AD. However, not all MCI cases advance; some remain stable (SMCI) or even revert to normal cognition, while others progress (PMCI) (Vecchio et al., 2018; Ge et al., 2025). Critically, many PMCI patients may already exhibit AD-related features at the time of data acquisition, although these are not identifiable without longitudinal follow-up, while some SMCI patients are closer to HC. This ambiguity makes certain MCI subjects difficult to distinguish from either AD or HC. Future work should therefore prioritize the collection of longitudinal EEG data to track disease progression.

Impact Statement

This paper introduces the first foundation model for EEG-based Alzheimer’s disease detection, trained on the largest EEG AD corpus available to date. Our results demonstrate that large-scale pre-trained models can substantially improve AD detection performance when appropriate training strategies and data curation are employed. The proposed approach significantly outperforms methods trained from scratch and existing SOTA EEG foundation models, even those trained on much larger EEG corpora. We hope that this work will advance research in EEG-based AD detection and inspire future studies on the detection of other brain disorders and neurodegenerative diseases. To facilitate further research, we release our pre-trained model checkpoints to support researchers with private EEG datasets for AD detection who face challenges in training robust models from scratch due to limited subject availability.

References

- Biosemi. URL <https://www.biosemi.com/index.htm>. Accessed: 2025-05-04.
- Abbaspourazad, S., Elachqar, O., Miller, A. C., Emrani, S., Nallasamy, U., and Shapiro, I. Large-scale training of foundation models for wearable biosignals. *The Twelfth International Conference on Learning Representations*, 2024.
- Ahmed, S., Momin, M., Ren, J., Lee, H., AlMahmood, B., Huang, L.-P., Pandiyani, A., Veeramuthu, L., Kuo, C.-C., and Zhou, T. Stick-and-play bioadhesive hair-like electrodes for chronic eeg recording on human. *npj Biomedical Innovations*, 2(1):9, 2025.
- Al-Nuaimi, A. H. H., Jammeh, E., Sun, L., and Ifeachor, E. Complexity measures for quantifying changes in electroencephalogram in alzheimer’s disease. *Complexity*, 2018(1):8915079, 2018.
- Alves, C. L., Pineda, A. M., Roster, K., Thielemann, C., and Rodrigues, F. A. Eeg functional connectivity and deep learning for automatic diagnosis of brain disorders: Alzheimer’s disease and schizophrenia. *Journal of Physics: complexity*, 3(2):025001, 2022.
- Amezquita-Sanchez, J. P., Mammone, N., Morabito, F. C., Marino, S., and Adeli, H. A novel methodology for automated differential diagnosis of mild cognitive impairment and the alzheimer’s disease using eeg signals. *Journal of neuroscience methods*, 322:88–95, 2019.
- Aviles, M., Sánchez-Reyes, L. M., Álvarez-Alvarado, J. M., and Rodríguez-Reséndiz, J. Machine and deep learning trends in eeg-based detection and diagnosis of alzheimer’s disease: A systematic review. *Eng*, 5(3):1464–1484, 2024.
- Azami, H., Arnold, S. E., Sanei, S., Chang, Z., Sapiro, G., Escudero, J., and Gupta, A. S. Multiscale fluctuation-based dispersion entropy and its applications to neurological diseases. *IEEE Access*, 7:68718–68733, 2019.
- Baevski, A., Zhou, Y., Mohamed, A., and Auli, M. wav2vec 2.0: A framework for self-supervised learning of speech representations. *Advances in neural information processing systems*, 33:12449–12460, 2020.
- Bai, S., Kolter, J. Z., and Koltun, V. An empirical evaluation of generic convolutional and recurrent networks for sequence modeling. *arXiv preprint arXiv:1803.01271*, 2018.
- Breijyeh, Z. and Karaman, R. Comprehensive review on alzheimer’s disease: Causes and treatment. *Molecules*, 25(24):5789, 2020.
- Cassani, R., Falk, T. H., Fraga, F. J., Kanda, P. A., and Anghinah, R. The effects of automated artifact removal algorithms on electroencephalography-based alzheimer’s disease diagnosis. *Frontiers in aging neuroscience*, 6:55, 2014.
- Cavanagh, F. Eeg: Depression rest. *OpenNeuro, Dataset*, 2021.
- Cavanagh, J. F., Bismark, A. W., Frank, M. J., and Allen, J. J. Multiple dissociations between comorbid depression and anxiety on reward and punishment processing: Evidence from computationally informed eeg. *Computational Psychiatry (Cambridge, Mass.)*, 3:1, 2019.
- Chen, T., Kornblith, S., Norouzi, M., and Hinton, G. A simple framework for contrastive learning of visual representations. In *International conference on machine learning*, pp. 1597–1607. PMLR, 2020.
- Chenot, Q., Hamery, C., Truninger, M., Langer, N., Scannella, S., et al. Investigating the relationship between resting-state eeg microstates and executive functions: A null finding. *cortex*, 178:1–17, 2024.
- Chu, L. Alzheimer’s disease: early diagnosis and treatment. *Hong Kong Medical Journal*, 18(3):228, 2012.
- Coronel, C., Garn, H., Waser, M., Deistler, M., Benke, T., Dal-Bianco, P., Ransmayr, G., Seiler, S., Grossegger, D., and Schmidt, R. Quantitative eeg markers of entropy and auto mutual information in relation to mmse scores of probable alzheimer’s disease patients. *Entropy*, 19(3): 130, 2017.

- Cui, W., Jeong, W., Thölke, P., Medani, T., Jerbi, K., Joshi, A. A., and Leahy, R. M. Neuro-gpt: Towards a foundation model for eeg. In 2024 IEEE International Symposium on Biomedical Imaging (ISBI), pp. 1–5. IEEE, 2024.
- Cura, O. K., Yilmaz, G. C., Ture, H. S., and Akan, A. Deep time-frequency feature extraction for alzheimer's dementia eeg classification. In 2022 Medical Technologies Congress (TIPEKNO), pp. 1–4. IEEE, 2022.
- Döner, B., Ingolfsson, T. M., Benini, L., and Li, Y. Luna: Efficient and topology-agnostic foundation model for eeg signal analysis. In 1st ICML Workshop on Foundation Models for Structured Data.
- Dzianok, P. and Kublik, E. Pearl-neuro database: Eeg, fmri, health and lifestyle data of middle-aged people at risk of dementia. Scientific Data, 11(1):276, 2024.
- Escudero, J., Abásolo, D., Hornero, R., Espino, P., and López, M. Analysis of electroencephalograms in alzheimer's disease patients with multiscale entropy. Physiological measurement, 27(11):1091, 2006.
- Fahimi, G., Tabatabaei, S. M., Fahimi, E., and Rajebi, H. Index of theta/alpha ratio of the quantitative electroencephalogram in alzheimer's disease: a case-control study. Acta Medica Iranica, pp. 502–506, 2017.
- Fan, W., Fei, J., Guo, D., Yi, K., Song, X., Xiang, H., Ye, H., and Li, M. Towards multi-resolution spatiotemporal graph learning for medical time series classification. In Proceedings of the ACM on Web Conference 2025, pp. 5054–5064, 2025.
- Fang, Z., Li, C., Zhou, H., Yu, S., Du, G., Qasem, A., Lu, Y., Li, J., Zhang, J., and Goh, S. K. Neuript: Foundation model for neural interfaces. arXiv preprint arXiv:2510.16548, 2025.
- Fraga, F. J., Falk, T. H., Kanda, P. A., and Anghinah, R. Characterizing alzheimer's disease severity via resting-awake eeg amplitude modulation analysis. PLoS one, 8(8):e72240, 2013.
- Gallego-Viñarás, L., Mira-Tomás, J. M., Gaeta, A. M., Pinol-Ripoll, G., Barbé, F., Olmos, P. M., and Muñoz-Barrutia, A. Alzheimer's disease detection in eeg sleep signals. IEEE Journal of Biomedical and Health Informatics, 2024.
- Garn, H., Waser, M., Deistler, M., Benke, T., Dal-Bianco, P., Ransmayr, G., Schmidt, H., Sanin, G., Santer, P., Caravias, G., et al. Quantitative eeg markers relate to alzheimer's disease severity in the prospective dementia registry austria (prodem). Clinical Neurophysiology, 126(3):505–513, 2015.
- Ge, Y., Yin, J., Chen, C., Yang, S., Han, Y., Ding, C., Zheng, J., Zheng, Y., and Zhang, J. An eeg-based framework for automated discrimination of conversion to alzheimer's disease in patients with amnesic mild cognitive impairment: an 18-month longitudinal study. Frontiers in Aging Neuroscience, 16:1470836, 2025.
- Getzmann, S., Gajewski, P. D., Schneider, D., and Wascher, E. Resting-state eeg data before and after cognitive activity across the adult lifespan and a 5-year follow-up. Scientific Data, 11(1):988, 2024.
- Gramfort, A., Luessi, M., Larson, E., Engemann, D. A., Strohmeier, D., Brodbeck, C., Goj, R., Jas, M., Brooks, T., Parkkonen, L., et al. Meg and eeg data analysis with mne-python. Frontiers in Neuroinformatics, 7:267, 2013.
- Grill, J.-B., Strub, F., Alché, F., Tallec, C., Richemond, P., Buchatskaya, E., Doersch, C., Avila Pires, B., Guo, Z., Gheshlaghi Azar, M., et al. Bootstrap your own latent: a new approach to self-supervised learning. Advances in neural information processing systems, 33:21271–21284, 2020.
- Hatlestad-Hall, C., Rygvold, T. W., and Andersson, S. Bids-structured resting-state electroencephalography (eeg) data extracted from an experimental paradigm. Data in Brief, 45:108647, 2022.
- He, K., Fan, H., Wu, Y., Xie, S., and Girshick, R. Momentum contrast for unsupervised visual representation learning. In Proceedings of the IEEE/CVF conference on computer vision and pattern recognition, pp. 9729–9738, 2020.
- He, K., Chen, X., Xie, S., Li, Y., Dollár, P., and Girshick, R. Masked autoencoders are scalable vision learners. In Proceedings of the IEEE/CVF conference on computer vision and pattern recognition, pp. 16000–16009, 2022.
- Homan, R. W., Herman, J., and Purdy, P. Cerebral location of international 10–20 system electrode placement. Electroencephalography and clinical neurophysiology, 66(4):376–382, 1987.
- Ieracitano, C., Mammone, N., Bramanti, A., Hussain, A., and Morabito, F. C. A convolutional neural network approach for classification of dementia stages based on 2d-spectral representation of eeg recordings. Neurocomputing, 323:96–107, 2019a.
- Ieracitano, C., Mammone, N., Bramanti, A., Marino, S., Hussain, A., and Morabito, F. C. A time-frequency based machine learning system for brain states classification via eeg signal processing. In 2019 International Joint Conference on Neural Networks (IJCNN), pp. 1–8. IEEE, 2019b.

- Jiang, W.-B., Wang, Y., Lu, B.-L., and Li, D. Neurolm: A universal multi-task foundation model for bridging the gap between language and eeg signals. *arXiv preprint arXiv:2409.00101*, 2024a.
- Jiang, W.-B., Zhao, L.-M., and Lu, B.-L. Large brain model for learning generic representations with tremendous eeg data in bci. *The Twelfth International Conference on Learning Representations*, 2024b.
- Kachare, P. H., Sangle, S. B., Puri, D. V., Khubrani, M. M., and Al-Shourbaji, I. Steadynet: spatiotemporal eeg analysis for dementia detection using convolutional neural network. *Cognitive Neurodynamics*, pp. 1–14, 2024.
- Kanda, P. A. M., Trambaiolli, L. R., Lorena, A. C., Fraga, F. J., Basile, L. F. I., Nitrini, R., and Anghinah, R. Clinician's road map to wavelet eeg as an alzheimer's disease biomarker. *Clinical EEG and neuroscience*, 45(2):104–112, 2014.
- Kim, M.-j., Youn, Y. C., and Paik, J. Deep learning-based eeg analysis to classify normal, mild cognitive impairment, and dementia: Algorithms and dataset. *NeuroImage*, 272:120054, 2023.
- Kiyasseh, D., Zhu, T., and Clifton, D. A. Clocs: Contrastive learning of cardiac signals across space, time, and patients. In *International Conference on Machine Learning*, pp. 5606–5615. PMLR, 2021.
- Klepl, D., He, F., Wu, M., Blackburn, D. J., and Sarriannian, P. Adaptive gated graph convolutional network for explainable diagnosis of alzheimer's disease using eeg data. *IEEE Transactions on Neural Systems and Rehabilitation Engineering*, 2023.
- Kostas, D., Aroca-Ouellette, S., and Rudzicz, F. Bendr: Using transformers and a contrastive self-supervised learning task to learn from massive amounts of eeg data. *Frontiers in Human Neuroscience*, 15:653659, 2021.
- Kulkarni, N. and Bairagi, V. Extracting salient features for eeg-based diagnosis of alzheimer's disease using support vector machine classifier. *IETE Journal of Research*, 63(1):11–22, 2017.
- Lahijanian, M., Aghajan, H., and Vahabi, Z. Auditory gamma-band entrainment enhances default mode network connectivity in dementia patients. *Scientific Reports*, 14(1):13153, 2024.
- Lawhern, V. J., Solon, A. J., Waytowich, N. R., Gordon, S. M., Hung, C. P., and Lance, B. J. Eegnet: a compact convolutional neural network for eeg-based brain-computer interfaces. *Journal of neural engineering*, 15(5):056013, 2018.
- Lea, C., Flynn, M. D., Vidal, R., Reiter, A., and Hager, G. D. Temporal convolutional networks for action segmentation and detection. In *proceedings of the IEEE Conference on Computer Vision and Pattern Recognition*, pp. 156–165, 2017.
- Li, F., Matsumori, S., Egawa, N., Yoshimoto, S., Yamashiro, K., Mizutani, H., Uchida, N., Kokuryu, A., Kuzuya, A., Kojima, R., et al. Predictive diagnostic approach to dementia and dementia subtypes using wireless and mobile electroencephalography: A pilot study. *Bioelectricity*, 4(1):3–11, 2022.
- Liu, D., Chen, Z., Luo, J., Lian, S., and Wu, D. Mirepnet: A pipeline and foundation model for eeg-based motor imagery classification. *arXiv preprint arXiv:2507.20254*, 2025.
- Liu, X., Zhang, C., Ji, Z., Ma, Y., Shang, X., Zhang, Q., Zheng, W., Li, X., Gao, J., Wang, R., et al. Multiple characteristics analysis of alzheimer's electroencephalogram by power spectral density and lempel–ziv complexity. *Cognitive neurodynamics*, 10:121–133, 2016.
- Liu, Y., Hu, T., Zhang, H., Wu, H., Wang, S., Ma, L., and Long, M. itransformer: Inverted transformers are effective for time series forecasting. *International conference on learning representations*, 2023a.
- Liu, Y., Hu, T., Zhang, H., Wu, H., Wang, S., Ma, L., and Long, M. itransformer: Inverted transformers are effective for time series forecasting. In *The Twelfth International Conference on Learning Representations*, 2023b.
- Luo, D. and Wang, X. Moderntcn: A modern pure convolution structure for general time series analysis. In *The twelfth international conference on learning representations*, pp. 1–43, 2024.
- Masters, C. L., Bateman, R., Blennow, K., Rowe, C. C., Sperling, R. A., and Cummings, J. L. Alzheimer's disease. *Nature reviews disease primers*, 1(1):1–18, 2015.
- Miltiadous, A., Gionanidis, E., Tzimourta, K. D., Giannakeas, N., and Tzallas, A. T. Dice-net: a novel convolution-transformer architecture for alzheimer detection in eeg signals. *IEEE Access*, 2023a.
- Miltiadous, A., Tzimourta, K. D., Afrantou, T., Ioannidis, P., Grigoriadis, N., Tsalikakis, D. G., Angelidis, P., Tsiouras, M. G., Glavas, E., Giannakeas, N., et al. A dataset of scalp eeg recordings of alzheimer's disease, frontotemporal dementia and healthy subjects from routine eeg. *Data*, 8(6):95, 2023b.

- Mohammadi Foumani, N., Mackellar, G., Ghane, S., Irtza, S., Nguyen, N., and Salehi, M. Eeg2rep: enhancing self-supervised eeg representation through informative masked inputs. In Proceedings of the 30th ACM SIGKDD Conference on Knowledge Discovery and Data Mining, pp. 5544–5555, 2024.
- Mora-Sánchez, A., Dreyfus, G., and Vialatte, F.-B. Scale-free behaviour and metastable brain-state switching driven by human cognition, an empirical approach. Cognitive neurodynamics, 13:437–452, 2019.
- National Academies of Sciences, Engineering, and Medicine. Reducing the impact of dementia in america: A decadal survey of the behavioral and social sciences. 2021.
- Nelson, L. and Tabet, N. Slowing the progression of alzheimer's disease; what works? Ageing research reviews, 23:193–209, 2015.
- Nie, Y. A time series is worth 64 words: Long-term forecasting with transformers. International conference on learning representations, 2023.
- Obeid, I. and Picone, J. The temple university hospital eeg data corpus. Frontiers in neuroscience, 10:196, 2016.
- Ouahidi, Y. E., Lys, J., Thölke, P., Farrugia, N., Pasdeloup, B., Gripon, V., Jerbi, K., and Lioi, G. Reve: A foundation model for eeg—adapting to any setup with large-scale pretraining on 25,000 subjects. arXiv preprint arXiv:2510.21585, 2025.
- Phalen, H., Coffman, B. A., Ghuman, A., Sejdić, E., and Salisbury, D. F. Non-negative matrix factorization reveals resting-state cortical alpha network abnormalities in the first-episode schizophrenia spectrum. Biological Psychiatry: Cognitive Neuroscience and Neuroimaging, 5(10):961–970, 2020.
- Pion-Tonachini, L., Kreutz-Delgado, K., and Makeig, S. Iclabel: An automated electroencephalographic independent component classifier, dataset, and website. NeuroImage, 198:181–197, 2019.
- Prado, P., Medel, V., Gonzalez-Gomez, R., Sainz-Ballesteros, A., Vidal, V., Santamaría-García, H., Moguilner, S., Mejia, J., Slachevsky, A., Behrens, M. I., et al. The brainlat project, a multimodal neuroimaging dataset of neurodegeneration from underrepresented backgrounds. Scientific Data, 10(1):889, 2023.
- Roncero-Parra, C., Parreño-Torres, A., Sánchez-Reolid, R., Mateo-Sotos, J., and Borja, A. L. Inter-hospital moderate and advanced alzheimer's disease detection through convolutional neural networks. Heliyon, 10(4), 2024.
- Schmidt, M. T., Kanda, P. A., Basile, L. F., da Silva Lopes, H. F., Baratho, R., Demario, J. L., Jorge, M. S., Nardi, A. E., Machado, S., Ianof, J. N., et al. Index of alpha/theta ratio of the electroencephalogram: a new marker for alzheimer's disease. Frontiers in aging neuroscience, 5: 60, 2013.
- Shan, X., Cao, J., Huo, S., Chen, L., Sarrigiannis, P. G., and Zhao, Y. Spatial-temporal graph convolutional network for alzheimer classification based on brain functional connectivity imaging of electroencephalogram. Human Brain Mapping, 43(17):5194–5209, 2022.
- Shor, O., Glik, A., Yaniv-Rosenfeld, A., Valevski, A., Weizman, A., Khrennikov, A., and Benninger, F. Eeg p-adic quantum potential accurately identifies depression, schizophrenia and cognitive decline. Plos one, 16(8): e0255529, 2021.
- Singh, A., Cole, R. C., Espinoza, A. I., Wessel, J. R., Cavanagh, J. F., and Narayanan, N. S. Evoked mid-frontal activity predicts cognitive dysfunction in parkinson's disease. Journal of Neurology, Neurosurgery & Psychiatry, 94(11):945–953, 2023.
- Song, Y., Zheng, Q., Liu, B., and Gao, X. Eeg conformer: Convolutional transformer for eeg decoding and visualization. IEEE Transactions on Neural Systems and Rehabilitation Engineering, 31:710–719, 2022.
- Tait, L., Stothart, G., Coulthard, E., Brown, J. T., Kazanina, N., and Goodfellow, M. Network substrates of cognitive impairment in alzheimer's disease. Clinical Neurophysiology, 130(9):1581–1595, 2019.
- Trambaiolli, L. R., Lorena, A. C., Fraga, F. J., Kanda, P. A., Anghinah, R., and Nitrini, R. Improving alzheimer's disease diagnosis with machine learning techniques. Clinical EEG and neuroscience, 42(3):160–165, 2011.
- Tylova, L., Kukul, J., and Vysata, O. Predictive models in diagnosis of alzheimer's disease from eeg. Acta Polytechnica, 53(2), 2013.
- Tylová, L., Kukul, J., Hubata-Vacek, V., and Vyšata, O. Unbiased estimation of permutation entropy in eeg analysis for alzheimer's disease classification. Biomedical Signal Processing and Control, 39:424–430, 2018.
- Tzamourta, K. D., Afrantou, T., Ioannidis, P., Karatzikou, M., Tzallas, A. T., Giannakeas, N., Astrakas, L. G., Angelidis, P., Glavas, E., Grigoriadis, N., et al. Analysis of electroencephalographic signals complexity regarding alzheimer's disease. Computers & Electrical Engineering, 76:198–212, 2019a.

- Tzimourta, K. D., Giannakeas, N., Tzallas, A. T., Astrakas, L. G., Afrantou, T., Ioannidis, P., Grigoriadis, N., Angelidis, P., Tsalikakis, D. G., and Tsipouras, M. G. Eeg window length evaluation for the detection of alzheimer's disease over different brain regions. *Brain sciences*, 9(4): 81, 2019b.
- Van Dijk, H., Van Wingen, G., Denys, D., Olbrich, S., Van Ruth, R., and Arns, M. The two decades brainclinics research archive for insights in neurophysiology (tdbrain) database. *Scientific data*, 9(1):333, 2022.
- Vecchio, F., Miraglia, F., Iberite, F., Lacidogna, G., Guglielmi, V., Marra, C., Pasqualetti, P., Tiziano, F. D., and Rossini, P. M. Sustainable method for alzheimer dementia prediction in mild cognitive impairment: Electroencephalographic connectivity and graph theory combined with apolipoprotein e. *Annals of neurology*, 84(2): 302–314, 2018.
- Veloso, L., McHugh, J., Von Weltin, E., Lopez, S., Obeid, I., and Picone, J. Big data resources for eegs: Enabling deep learning research. In *2017 IEEE Signal Processing in Medicine and Biology Symposium (SPMB)*, pp. 1–3. IEEE, 2017.
- Vicchietti, M. L., Ramos, F. M., Betting, L. E., and Campanharo, A. S. Computational methods of eeg signals analysis for alzheimer's disease classification. *Scientific Reports*, 13(1):8184, 2023.
- Wang, G., Liu, W., He, Y., Xu, C., Ma, L., and Li, H. Eegpt: Pretrained transformer for universal and reliable representation of eeg signals. *Advances in Neural Information Processing Systems*, 2024a.
- Wang, J., Fang, Y., Wang, X., Yang, H., Yu, X., and Wang, H. Enhanced gamma activity and cross-frequency interaction of resting-state electroencephalographic oscillations in patients with alzheimer's disease. *Frontiers in aging neuroscience*, 9:243, 2017.
- Wang, J., Zhao, S., Luo, Z., Zhou, Y., Jiang, H., Li, S., Li, T., and Pan, G. Cbramod: A criss-cross brain foundation model for eeg decoding. *ICLR*, 2025.
- Wang, R., Wang, J., Li, S., Yu, H., Deng, B., and Wei, X. Multiple feature extraction and classification of electroencephalograph signal for alzheimers' with spectrum and bispectrum. *Chaos: An Interdisciplinary Journal of Nonlinear Science*, 25(1), 2015.
- Wang, Y., Han, Y., Wang, H., and Zhang, X. Contrast everything: A hierarchical contrastive framework for medical time-series. *Advances in Neural Information Processing Systems*, 36:55694–55717, 2023.
- Wang, Y., Huang, N., Li, T., Yan, Y., and Zhang, X. Medformer: A multi-granularity patching transformer for medical time-series classification. *Advances in Neural Information Processing Systems*, 2024b.
- Wang, Y., Mammone, N., Petrovsky, D., Tzallas, A. T., Morabito, F. C., and Zhang, X. Adformer: A multi-granularity transformer for eeg-based alzheimer's disease assessment. *arXiv preprint arXiv:2409.00032*, 2024c.
- Waser, M., Deistler, M., Garn, H., Benke, T., Dal-Bianco, P., Ransmayr, G., Grosseegger, D., and Schmidt, R. Eeg in the diagnostics of alzheimer's disease. *Statistical Papers*, 54:1095–1107, 2013.
- Waser, M., Garn, H., Schmidt, R., Benke, T., Dal-Bianco, P., Ransmayr, G., Schmidt, H., Seiler, S., Sanin, G., Mayer, F., et al. Quantifying synchrony patterns in the eeg of alzheimer's patients with linear and non-linear connectivity markers. *Journal of Neural Transmission*, 123:297–316, 2016.
- Watanabe, Y., Miyazaki, Y., Hata, M., Fukuma, R., Aoki, Y., Kazui, H., Araki, T., Taomoto, D., Satake, Y., Suehiro, T., et al. A deep learning model for the detection of various dementia and mci pathologies based on resting-state electroencephalography data: A retrospective multicentre study. *Neural Networks*, 171:242–250, 2024.
- Wu, D., Li, S., Yang, J., and Sawan, M. Neuro-bert: Rethinking masked autoencoding for self-supervised neurological pretraining. *IEEE Journal of Biomedical and Health Informatics*, 2024.
- Wu, H., Hu, T., Liu, Y., Zhou, H., Wang, J., and Long, M. Timesnet: Temporal 2d-variation modeling for general time series analysis. *arXiv preprint arXiv:2210.02186*, 2022.
- Wu, H., Hu, T., Liu, Y., Zhou, H., Wang, J., and Long, M. Timesnet: Temporal 2d-variation modeling for general time series analysis. In *International Conference on Learning Representations*, 2023.
- Wu, Z., Xiong, Y., Yu, S. X., and Lin, D. Unsupervised feature learning via non-parametric instance discrimination. In *Proceedings of the IEEE conference on computer vision and pattern recognition*, pp. 3733–3742, 2018.
- Xu, Q.-S. and Liang, Y.-Z. Monte carlo cross validation. *Chemometrics and Intelligent Laboratory Systems*, 56(1):1–11, 2001.
- Yang, C., Westover, M., and Sun, J. Biot: Biosignal transformer for cross-data learning in the wild. *Advances in Neural Information Processing Systems*, 36, 2024.

- Yuan, Z., Zhang, D., Yang, Y., Chen, J., and Li, Y. Ppi: Pretraining brain signal model for patient-independent seizure detection. Advances in Neural Information Processing Systems, 36:69586–69604, 2023.
- Yue, T., Xue, S., Gao, X., Tang, Y., Guo, L., Jiang, J., and Liu, J. Eegpt: Unleashing the potential of eeg generalist foundation model by autoregressive pre-training. arXiv preprint arXiv:2410.19779, 2024.
- Zhang, C., Kim, Y.-K., and Eskandarian, A. Eeg-inception: an accurate and robust end-to-end neural network for eeg-based motor imagery classification. Journal of Neural Engineering, 18(4):046014, 2021.
- Zhang, D., Yuan, Z., Yang, Y., Chen, J., Wang, J., and Li, Y. Brant: Foundation model for intracranial neural signal. Advances in Neural Information Processing Systems, 36: 26304–26321, 2023.
- Zhou, Y., Wu, J., Ren, Z., Yao, Z., Lu, W., Peng, K., Zheng, Q., Song, C., Ouyang, W., and Gou, C. Csbrain: A cross-scale spatiotemporal brain foundation model for eeg decoding. arXiv preprint arXiv:2506.23075, 2025.
- Zhu, Q., Zhao, X., Zhang, J., Gu, Y., Weng, C., and Hu, Y. Eeg2vec: Self-supervised electroencephalographic representation learning. arXiv preprint arXiv:2305.13957, 2023.

A. Related Work

A.1. EEG-Based AD Detection

In the last two decades, EEG-based AD detection has followed two main research directions: manual biomarker extraction and deep learning representation.

Manual Biomarker Extraction: This research direction aims to identify potential biomarkers in EEG signals of AD patients and use simple classifiers, such as Multi-Layer Perceptrons (MLP) and Support Vector Machines (SVM), to differentiate these features from normal healthy subjects. Different types of EEG features are used, including statistical features like Mean, Skewness, Kurtosis, and Standard Deviation (Tzimourta et al., 2019b;a; Kulkarni & Bairagi, 2017; Kanda et al., 2014; Waser et al., 2013; Tylova et al., 2013; Mora-Sánchez et al., 2019), spectral features like Phase Shift, Phase Coherence, Bispectrum, and Bicoherence (Wang et al., 2017; Cassani et al., 2014; Wang et al., 2015; Fraga et al., 2013; Tait et al., 2019; Waser et al., 2016; Trambaiolli et al., 2011), power features like Power Spectrum Density, Relative Band Power, Ratio of EEG Rhythm, and Energy (Fahimi et al., 2017; Schmidt et al., 2013; Liu et al., 2016; Kanda et al., 2014), as well as complexity features like Shannon Entropy, Tsallis Entropy, and Permutation Entropy (Garn et al., 2015; Azami et al., 2019; Tylová et al., 2018; Coronel et al., 2017; Al-Nuaimi et al., 2018). The main advantage of this approach is its interpretability, but it suffers from limited performance.

Deep Learning: Compared to manual biomarker extraction, deep learning offers an alternative approach by automatically extracting useful representations for AD detection. Models such as Convolutional Neural Networks (CNNs) (Li et al., 2022; Cura et al., 2022), Graph Neural Networks (GNNs) (Shan et al., 2022; Klepl et al., 2023), and Transformers (Wang et al., 2024c) are widely used for representation learning. Some researchers still perform manual feature extraction or transform the data before applying deep learning models. For example, the method in (Ieracitano et al., 2019a) converts 5-second EEG intervals into Power Spectral Density (PSD) images and uses 2D convolutional layers on the images for feature extraction. DICE-net (Miltiadous et al., 2023a) extracts relative band power and spectral coherence connectivity across five frequency bands and applies convolutional layers followed by transformers. In contrast, some studies apply deep learning methods directly to EEG data. For instance, the method in (Gallego-Viñarás et al., 2024) uses semi-supervised spatiotemporal representation learning with deep learning models for AD detection based on different sleep-stage EEG data. STEADYNet (Kachare et al., 2024) designs low-complexity convolutional models for AD and dementia detection, focusing on fast inference times. Research in (Watanabe et al., 2024) using MNet that applies convolutional networks for feature extraction and

concatenates with the relative power spectrum for AD and other dementia detection. ADformer (Wang et al., 2024c) uses a multi-granularity transformer for AD detection and widely tests on 4 AD datasets.

A.2. Self-Supervised and Foundation Model in EEG

Two main strategies are widely used for self-supervised representation learning and foundation model training in EEG: contrastive learning and mask-reconstruction.

Contrastive Learning: BENDR (Kostas et al., 2021) follows a similar contrastive learning pipeline as Wav2Vec (Baeovski et al., 2020), but it is trained on EEG data. EEG2Vec (Zhu et al., 2023) explores both contrastive learning and mask-reconstruction for self-supervised pre-training on EEG data. BIOT (Yang et al., 2024) designs a transformer architecture for biomedical signal embedding and applies a self-supervised contrastive framework similar to BYOL (Grill et al., 2020). COMET (Wang et al., 2023) utilizes various data levels in biomedical time series to define positive and negative pairs.

Mask-Reconstruction: Neuro-BERT (Wu et al., 2024) employs masked autoencoding to predict missing amplitude and phase of EEG signals during pre-training. EEG2Rep (Mohammadi Foumani et al., 2024) combines a context encoder with a momentum target encoder to reconstruct context-level representations rather than raw data in self-supervised pre-training. LaBraM (Jiang et al., 2024b), the first large foundation model in the EEG domain, uses a neural tokenizer to reconstruct the Fourier spectrum during self-supervised pre-training. EEGPT (Wang et al., 2024a) is a foundation model for EEG representation learning that integrates reconstruction loss with an alignment loss between the encoder and momentum encoder. CBraMod (Wang et al., 2025) designs a criss-cross transformer to leverage both spatial and temporal features of EEG. LUNA (Döner et al.) introduces a cross-attention mechanism for a topology-agnostic foundation model capable of handling heterogeneous channels. CSBrain (Zhou et al., 2025) utilizes regions of the brain to design cross-window and cross-region dependencies for diverse decoding EEG tasks. NeurIPT (Fang et al., 2025) leverages a progressive mixture-of-experts architecture to build backbones and introduces 3D electrode embedding for EEG channel embedding. REVE (Ouahidi et al., 2025) pretrains on over 60,000 hours of EEG data from 92 datasets spanning 25,000 subjects, demonstrating the world’s largest EEG pre-training resources so far.

Other Strategies. Recent work has begun exploring autoregressive pre-training for EEG, such as NeuroGPT (Cui et al., 2024) and a study also named EEGPT (Yue et al., 2024). Research bridging language and EEG has also emerged, for instance, NeuroLM (Jiang et al., 2024a), which treats EEG as a foreign language for representation learning.

Application-Oriented Approaches. Several studies focus on application-specific foundation models. Brant (Zhang et al., 2023) trains a model tailored to intracranial neural signals; PPI (Yuan et al., 2023) develops a self-supervised framework for subject-independent seizure detection; MIRepNet (Liu et al., 2025) designs a foundation model for motor imagery classification.

B. Brain Diseases Detection with EEG

Neurological disease detection using EEG typically involves assigning a single label to each subject, reflecting their physiological brain state at the time of data acquisition, such as the presence or absence of AD (Conditions like seizures involve episodic labeling are not considered here). This assumes that a subject’s state remains stable during the relatively short recording period (e.g., several days), meaning all data from that subject shares the same label. Exceptions arise with longitudinal datasets that track disease progression (e.g., Healthy \rightarrow Mild Cognitive Impairment (MCI) \rightarrow AD (Vecchio et al., 2018; Ge et al., 2025)); in such cases, trials/sessions reflecting a change in diagnosis for the same subject are treated as different subjects during training. Besides, comorbid neurological conditions are often reported in brain disorders such as dementia. For instance, a patient may present with both AD and Vascular Dementia (VD) (Kim et al., 2023). This introduces an inherently multi-label scenario, in which each brain condition should be predicted independently via a dedicated projection head formulated as a binary classification task.

C. Self-Supervised Contrastive Losses

EEG, as a type of medical time series, contains more hierarchical structures than general time series data, such as session and subject ID information. Effective pre-training strategies can leverage this information to guide the design of EEG-specific representation learning frameworks under appropriate assumptions. In this work, we utilize two contrastive modules, **sample-level** and **subject-level** contrasting, as defined in COMET (Wang et al., 2023).

Representation Learning. For an input EEG sample x_i , where i denotes the sample index, we apply two data augmentations a and b to generate two distinct views x_i^a and x_i^b . Given a backbone encoder $f(\cdot)$ and a projection head $g(\cdot)$, we first compute intermediate representations via the encoder $h_i^a = f(x_i^a)$, $h_i^b = f(x_i^b)$. These are then passed through the projection head to obtain denser representations $z_i^a = g(h_i^a)$, $z_i^b = g(h_i^b)$ for self-supervised pre-training.

Sample-Level Contrasting. Sample-level contrastive learning treats different augmented views of the same sample as positive pairs, and views from different samples as neg-

ative pairs. This instance discrimination framework is widely used in contrastive learning, as demonstrated in SimCLR (Chen et al., 2020) and MoCo (He et al., 2020), and helps the model learn general representations from unlabeled EEG data (Wu et al., 2018). The sample-level contrastive loss \mathcal{L}_{co}^{sam} is defined as:

$$\mathcal{L}_{co}^{sam} = \mathbb{E}_{x_i} \left[-\log \frac{\exp(\text{sim}(z_i^a, z_i^b)/\tau)}{\sum_j (\exp(\text{sim}(z_i^a, z_j^b)/\tau))} \right] \quad (11)$$

where j indexes all other samples in the batch \mathcal{B} , and $\text{sim}(\mathbf{u}, \mathbf{v}) = \frac{\mathbf{u}^\top \mathbf{v}}{\|\mathbf{u}\| \|\mathbf{v}\|}$ denotes cosine similarity. The temperature parameter τ controls the sharpness of the distribution.

Subject-Level Contrasting. In EEG-based AD detection, each subject is generally associated with a stable pathological brain state in a short period, as discussed in section B. Once a subject is diagnosed with AD or exhibits early signs, all EEG segments from that subject are expected to share similar disease-relevant features. This assumption aligns naturally with subject-level contrasting, a framework defined by (Wang et al., 2023) and demonstrated to be effective in various EEG- and ECG-based disease detection tasks (Kiyasseh et al., 2021; Abbaspourazad et al., 2024). In this setting, samples from the same subject are considered positive pairs, and those from different subjects are considered negative. The subject-level contrastive loss \mathcal{L}_{co}^{sub} is defined as:

$$\mathcal{L}_{co}^{sub} = \mathbb{E}_{x_i} \left[\mathbb{E}_{x_k} \left[-\log \frac{\exp(\text{sim}(z_i^a, z_k^b)/\tau)}{\sum_j (\exp(\text{sim}(z_i^a, z_j^b)/\tau))} \right] \right] \quad (12)$$

where x_k denotes a sample in the batch sharing the same subject ID as x_i , i.e., $s_k = s_i$.

Overall Loss Function. The total self-supervised pre-training objective combines both contrastive losses as a weighted sum $\mathcal{L}_{co} = \lambda_1 \mathcal{L}_{co}^{sam} + \lambda_2 \mathcal{L}_{co}^{sub}$, where $\lambda_1 + \lambda_2 = 1$, and $\lambda_1, \lambda_2 \in [0, 1]$ control the relative importance of each loss component.

D. Data Augmentation Banks

For contrastive pre-training, we employ a bank of data augmentation methods to enhance the model’s robustness and generalization capabilities. During the forward pass in the training of each iteration, one augmentation method will be picked from available augmentation options with equal probability. The data augmentation methods include temporal flipping, temporal masking, frequency masking, channel

masking, jittering, and dropout, and can be further expanded to more choices.

1) Temporal Flipping. We reverse the EEG data along the temporal dimension. The probability of applying this augmentation is controlled by a parameter *prob*, with a default value of 0.5. **2) Temporal Masking.** We randomly mask timestamps across all channels. The proportion of timestamps masked is controlled by the parameter *ratio*, with a default value of 0.1. **3) Frequency Masking.** This method involves converting the EEG data into the frequency domain, randomly masking some frequency bands, and then converting it back. The proportion of frequency bands masked is controlled by the parameter *ratio*, with a default value of 0.1. **4) Channel Masking.** We randomly mask channels across all timestamps. The proportion of channel masked is controlled by the parameter *ratio*, with a default value of 0.1. **5) Jittering.** Random noise, ranging from 0 to 1, is added to the raw data. The intensity of the noise is adjusted by the parameter *scale*, which is set by default to 0.1. **6) Dropout.** Similar to the dropout layer in neural networks, this method randomly drops some values. The proportion of values dropped is controlled by the parameter *ratio*, with a default value of 0.1.

E. Implementation Details

Manual Feature utilize 32 features, including mean, variance, skewness, kurtosis, std, iqr, max, min, mean, median, delta power, theta power, alpha power, beta power, total power, theta alpha ratio, alpha beta ratio, delta relative power, theta relative power, alpha relative power, beta relative power, phase coherence, spectral centroid, spectral rolloff, spectral peak, average magnitude, median frequency, amplitude modulation, spectral entropy, tsallis entropy, and shannon entropy (Tzamourta et al., 2019b;a; Kulkarni & Bairagi, 2017; Kanda et al., 2014; Waser et al., 2013; Tylova et al., 2013; Mora-Sánchez et al., 2019; Wang et al., 2017; Cassani et al., 2014; Wang et al., 2015; Fraga et al., 2013; Tait et al., 2019; Waser et al., 2016; Trambaiolli et al., 2011; Fahimi et al., 2017; Schmidt et al., 2013; Liu et al., 2016; Kanda et al., 2014; Garn et al., 2015; Tylová et al., 2018; Coronel et al., 2017; Al-Nuaimi et al., 2018). A linear projection layer is then applied to these manually extracted features for final classification. Total parameters: 1,180.

EEGConformer (Song et al., 2022) uses convolutional modules to learn low-level local features and embed the raw data into patches for self-attention. We set $e_layers = 12$, $n_heads = 8$, $d_model = 128$, and $d_ff = 256$. Total parameters: 1,926,146.

EEGInception (Zhang et al., 2021) uses different scales of convolutional kernels, combined with a spatial block for feature extraction. We set $n_blocks = 3$, $channels =$

$(96,192,384)$, $kernel_sizes = (8,16,32)$, $depth_multiplier = 2$, $bottleneck_channels = 32$. Total parameters: 803,106.

EEGNet (Lawhern et al., 2018) is a classic deep learning method for EEG decoding. It uses depthwise and separable convolutions to capture spatial and temporal features. We keep the same structure when applying convolutions, normalization, and activations as described in the paper. Total parameters: 2,226.

iTransformer (Liu et al., 2023a) proposes a novel data-embedding method based on the transformer architecture for multivariate time-series analysis. It reverses the conventional embedding strategy. Instead of using multi-channel samples at a single time point into a single temporal token, iTransformer treats each channel/ivariate as an independent variable token. We set $e_layers = 12$, $n_heads = 8$, $d_model = 128$, and $d_ff = 256$. Total parameters: 1,607,810.

MedGNN (Fan et al., 2025) is a graph-nerual-network-based method for medical time-series classification. It uses a multi-resolution graph transformer architecture to model the dynamic dependencies and fuse the information from different resolutions. We set $-resolution_list = 2,4,6,8$, $-nodedim = 10$, $e_layers = 12$, $n_heads = 8$, $d_model = 128$, and $d_ff = 256$. Total parameters: 4,228,386.

Medformer (Wang et al., 2024b) is designed for biomedical time series classification, including EEG and ECG. Cross-channel multi-granularity patch embedding and intra-inter-granularity self-attention are utilized. We extended our work based on this method. We set $e_layers = 12$, $d_model = 128$, and $d_ff = 256$, $patch_len_list = [5, 10, 20]$. Total parameters: 4,851,202.

MNet (Watanabe et al., 2024) is a convolution-based deep learning method for EEG-based AD detection. It contains 4 Con2D blocks for feature extraction. We keep the same structure and order when applying convolutions, normalization, and activations as described in the paper. Total parameters: 1,980,738.

ModernTCN (Luo & Wang, 2024) is a convolutional architecture designed for general time-series analysis and demonstrates strong performance, particularly in classification. It combines depthwise convolutions with multiple pointwise convolutions and introduces channel-independent embedding mechanisms. We set $patch_len = 20$, $stride = 10$, $num_blocks = 1\ 1\ 1\ 1$, $large_size = 9\ 9\ 9\ 9$, $small_size = 5\ 5\ 5\ 5$, $dims = 32\ 64\ 128\ 128$. Total parameters: 1,906,210.

PatchTST (Nie, 2023) is a transformer-based model for time series prediction and representation learning, with its core innovation lying in a dual design of patching and channel independence. The model decomposes multi-channel data into multiple one-channel patches, treating them as semantically informative sub-sequence fragments for input.

We set $e_layers = 12$, $n_heads = 8$, $d_model = 128$, and $d_ff = 256$, $patch_len = 25$. Total parameters: 1,607,810.

TCN (Lea et al., 2017) is a convolutional architecture designed explicitly for time-series modeling. They extend residual networks by incorporating causal and dilated convolutions, enabling effective learning of long-range temporal dependencies. We set $e_layers = 12$, $n_heads = 8$, $d_model = 128$, and $d_ff = 256$. Total parameters: 1,024,706.

TimesNet (Wu et al., 2022) is a convolutional model for time-series analysis, especially on classification tasks. It transforms one-dimensional time-series data into two-dimensional tensors across multiple periodicities, thereby leveraging the strengths of 2D convolutional networks for time-series analysis. We set $e_layers = 2$, $top_k = 3$, $d_model = 32$, and $d_ff = 64$. Total parameters: 2,352,482.

BIOT (Yang et al., 2024) is the first foundation model for biomedical time-series data, including EEG. It employs single-channel patch embedding to handle biosignals with varying channel counts. Each patch is mapped to tokens, with segment, channel, and positional embeddings added to make the tokens distinguishable. To align the channel configuration of our datasets with their checkpoints, we use a 1D convolution (Conv1D) for channel mapping. We retain the other default architectural parameters from the checkpoint. The pre-trained checkpoint is available at <https://github.com/ycq091044/BIOT/blob/main/pretrained-models/EEG-PREST-16-channels.ckpt>. Total parameters: 3,187,544.

LaBraM (Jiang et al., 2024b) is the first EEG foundation model, trained on 2,000 hours of EEG recordings collected from multiple datasets. Its pre-training follows a two-step strategy that combines vector quantization with mask-based reconstruction. In our experiments, we use their released pre-trained checkpoint with default parameters and fine-tune it on four AD downstream datasets. To align the channel configuration of our datasets with their checkpoints, we use a 1D convolution (Conv1D) for channel mapping. We retain the other default architectural parameters from the checkpoint. The pre-trained checkpoint is available at <https://github.com/935963004/LaBraM/blob/main/checkpoints/labram-base.pth>. Total parameters: 5,822,770.

CBraMod (Wang et al., 2025) is an SOTA EEG foundation model trained on the 9000 hours TUEG dataset with 19 standard channels of the 10-20 system. They use a criss-cross transformer to perform spatial and temporal attention to capture features along two dimensions. We keep their default parameters to load their pre-trained checkpoint and fine-tune on 5 AD downstream datasets. The pre-trained checkpoint is available at https://huggingface.co/weighting666/CBraMod/blob/main/pretrained_weights.pth. Total parameters: 8,085,563.

CSBrain (Zhou et al., 2025) is an SOTA EEG foundation model that leverages brain regions to model cross-window and cross-region dependencies for diverse EEG decoding tasks. This model is also trained on the 9000 hours TUEG dataset with 19 standard channels of the 10-20 system. We keep their default parameters to load their pre-trained checkpoint and fine-tune on 5 AD downstream datasets. The pre-trained checkpoint is available at <https://drive.google.com/drive/folders/1je-1TtdHv6klcd-kTIPNkiA1wLrxybva>. Total parameters: 12,063,202.

LEAD (Ours). We pre-train on 13 datasets (4 AD and 9 Non-AD) and then fine-tune on 5 downstream AD datasets. We set the patch length L to 50 and the stride to 50. The sample- and subject-level cross-entropy loss weights α and β are both set to 0.5. The contrastive loss coefficients λ_1 and λ_2 are set to 0.25 and 0.75. We set $e_layers = 12$, $n_heads = 8$, $d_model = 128$, $d_ff = 256$, and $group_size = 8$. The indices group shuffling, sampling rate embedding, and multi-sampling segmentation are all enabled, with $multi_sampling_rate$ set to 200, 100, and 50 Hz. The $montage_name$ is set to *standard_1005*, and $channel_names$ are exactly matched with the channel configuration of the downstream dataset. Total parameters: 3,322,498.

F. Datasets Preprocessing

F.1. Data Curation

We categorize all EEG datasets utilized in this paper into two groups: those containing Alzheimer’s Disease subjects (**AD** datasets) and those without (**Non-AD** datasets).

AD Datasets. Despite the promise of EEG for AD detection, the field remains critically limited by the scarcity of accessible datasets. To address this, we conducted a comprehensive review of relevant publications and public EEG repositories (e.g., OpenNeuro, Dryad, figshare) published before 2026. This effort identified 8 public datasets. In total, we utilize 8 public and 1 private AD datasets, most of which consist of resting-state recordings, with minor evoked steady-state response: **AD-Auditory** (Lahijanani et al., 2024), **BrainLat** (Prado et al., 2023), **P-ADIC** (Shor et al., 2021), **CAUEEG** (Kim et al., 2023), **ADFSU** (Vicchiotti et al., 2023), **ADFTD** (Miltiadous et al., 2023b), **ADSZ** (Alves et al., 2022), **APAVA** (Escudero et al., 2006), and **CNBPM** (Amezquita-Sanchez et al., 2019). Together, these datasets comprise **2,238 subjects and 427.81 hours** of recordings, forming the **world’s largest** EEG-AD corpus reported so far.

Non-AD Datasets. While the inclusion of AD datasets represents a major step forward, their scale is still limited for large-scale pre-training, and a portion must be reserved for downstream evaluation. To further expand our training resources, we curated 9 **domain-relevant** non-AD datasets.

Table 6. Dataset Statistics. All datasets are downsampled to 200Hz, 100Hz, 50Hz, or a subset of them using multi-sampling segmentation. Each sample contains either 400, 200, or 100 timesteps after segmentation, corresponding to 4, 2, or 1 seconds at a sampling rate of 100Hz. All pre-training datasets are aligned to 19 channels, and the fine-tuning datasets keep the raw channel. The **h** and **m** in the total time column represent hours and minutes. Abbreviations: **ASSR**: Auditory Steady-State Response; **RS**: Resting State; **HV**: Hyperventilation; **PS**: Photic Stimulation. **HC** - Healthy Controls; **AD**: Alzheimer’s Disease; **FTD**: Frontotemporal Dementia; **PD**: Parkinson’s disease; **MS**: Multiple Sclerosis; **MCI**: Mild Cognitive Impairment; **SCZ**: Schizophrenia; **DEP**: Depression; **DEM**: Dementia; **FEP**: First Episode Psychosis; **MDD**: Major Depressive Disorder; **ADHD**: Attention Deficit Hyperactivity Disorder; **SMC**: Subjective Memory Complaints; **OCD**: Obsessive-Compulsive Disorder.

Category	Datasets	Paradigm	#Subjects	Sampling Rate	#Channels	Total Time	#Timestamps	#Samples	Classes	Tasks
Non-AD	BACA-RS	RS	608	1000→200,100,50 Hz	65→19	169.80h	400	1,057,775	HC	Pre-train
	Depression	RS	122	500→200,100,50 Hz	66→19	23.36h	400	146,062	HC, DEP	Pre-train
	FEP-PCR	RS	143	1000→200,100,50 Hz	64→19	12.27h	400	76,694	HC, FEP	Pre-train
	MCEF-RS	RS	165	512→200,100,50 Hz	64→19	14.14h	400	88,411	HC	Pre-train
	PD-RS	RS	149	500→200,100,50 Hz	60→19	6.64h	400	41,174	HC, PD	Pre-train
	PEARL-Neuro	RS	79	1000→200,100,50 Hz	127→19	14.36h	400	90,147	HC	Pre-train
	SRM-RS	RS	109	1024→200,100,50 Hz	64→19	9.10h	400	56,880	HC	Pre-train
	TDBrain	RS	1273	500→200,100,50 Hz	33→19	89.71h	400	555,455	MDD, ADHD, SMC, OCD, etc.	Pre-train
	TUEP	RS	200	256→200,100,50 Hz	21, etc.→19	466.24h	400	2,930,241	HC, Epilepsy	Pre-train
AD-Auditory	AD-Auditory	ASSR	35	250→200,100,50 Hz	19	5.20h	400	32,655	HC, AD, MCI	Pre-train
	BrainLat	RS	135	512→200,100,50 Hz	19	17.26h	400	108,206	HC, AD, FTD, PD, MS	Pre-train
	P-ADIC	RS	249	500→200,100,50 Hz	19	75.39h	400	473,970	HC, AD, MCI, SCZ, DEP	Pre-train
	CAUEEG	RS, PS, HV, etc.	1379	200→200,100,50 Hz	19	282.37h	400	1,773,814	HC, MCI, DEM, etc.	Pre-train
	AD	ADFSU	RS	92	128→100,50 Hz	19	24.53m	100	4048	HC, AD
ADFTD		RS, PS	88	500→200,100,50 Hz	19	26.64h	400	167,083	HC, AD, FTD	Fine-tune
ADSZ		RS	48	128→100,50 Hz	19	6.80m	100	1128	HC, AD	Fine-tune
APAVA		RS	23	256→200,100,50 Hz	16	0.92h	200	9282	HC, AD	Fine-tune
CNBPM		RS	189	256→200,100,50 Hz	19	19.51h	400	122,029	HC, MCI, AD	Fine-tune

Unlike existing EEG foundation models that mix paradigms such as resting-state (RS), motor imagery (MI), and event-related potentials (ERP) (Jiang et al., 2024b; Wang et al., 2024a), we deliberately focus on datasets aligned with AD detection. This decision is motivated by the fact that different paradigms reflect distinct neuroscientific processes and cortical activations, usually requiring paradigm-specific preprocessing pipelines. Combining data from heterogeneous paradigms can introduce conflicting patterns and diminish the utility of pre-training resources. Our curated non-AD datasets contain recordings from both healthy subjects and patients with other brain disorders (e.g., PD, DEP, ADHD). Specifically, we include: **BACA-RS** (Getzmann et al., 2024), **Depression** (Cavanagh et al., 2019), **FEP-PCR** (Phalen et al., 2020), **MCEF-RS** (Chenot et al., 2024), **PD-RS** (Singh et al., 2023), **PEARL-Neuro** (Dzianok & Kublik, 2024), **SRM-RS** (Hatlestad-Hall et al., 2022), **TDBrain** (Van Dijk et al., 2022), and **TUEP** (Veloso et al., 2017). Collectively, they comprise **2,848 subjects and 805.62 hours** of EEG. Most of these datasets were acquired under resting-state or resting-state-like paradigms, ensuring consistency with our downstream AD detection.

F.2. Unified Data Preprocessing

The statistics of processed datasets are provided in Table 6. The datasets are highly heterogeneous, with substantial variability in channel numbers, sampling rates, and recording lengths. To utilize them for training, we apply the following

preprocessing pipeline, applied sequentially:

- 1) Removal of non-EEG channels:** All non-EEG channels are removed, such as EOG, ECG, or coordinate information.
- 2) Notch and Band-Pass Filtering:** Each trial undergoes a notch filter at 50 Hz or 60 Hz, followed by a band-pass filter between 0.5 Hz and 45 Hz. This step aims to suppress line noise, slow drifts, and high-frequency noise, which are generally outside the frequency range of scalp-recorded brain activity.
- 3) Average re-referencing:** Average re-referencing is applied to reduce global noise and potential baseline shifts.
- 1) Artifact Removal:** For datasets lacking prior artifact rejection, we utilize independent component analysis (ICA) combined with the ICLabel algorithm (Pion-Tonachini et al., 2019) to automatically identify and remove components associated with artifacts like eye blinks, or muscle activity.
- 2) Channel Alignment:** We align all pre-training datasets (downstream datasets could be an arbitrary number of channels and montage) to the standard 19-channel montage based on the international 10-20 system: Fp1, Fp2, F7, F3, Fz, F4, F8, T3/T7, C3, Cz, C4, T4/T8, T5/P7, P3, Pz, P4, T6/P8, O1, and O2 (Homan et al., 1987). If a dataset has more channels, only the 19 channels with these names are selected, and the rest are discarded. For datasets employing different montages (e.g., Biosemi (bio)), signals are projected onto the target 19 channels using their 3D coordinates. All the fine-tuning datasets keep the raw channel.
- 3) Frequency Alignment:** All datasets are resampled to a uniform sampling frequency of 200 Hz. This rate is widely used, adequately

captures the main physiological EEG frequency bands (δ , θ , α , β , γ), and reduces high-frequency noise. **4) Data Segmentation:** We propose a novel **multi-sampling segmentation** strategy. Instead of resampling all EEG signals to a single fixed sampling rate, we downsample each recording to multiple sampling rates. Specifically, signals with an original sampling rate above 200 Hz are downsampled to 200, 100, and 50 Hz, while those with lower sampling rates are downsampled to 100 and 50 Hz. These three choices could cover almost all sampling rates in scalp EEG datasets. The resulting 200 Hz, 100 Hz, and 50 Hz signals are then segmented into half-overlapping windows of 100, 200, or 400 timestamps, corresponding to 1-second, 2-second, or 4-second segments if at a sampling rate of 100 Hz. Segments shorter than 200 or 400 timestamps at the boundaries of each trial are discarded. This segmentation strategy naturally enables multi-scale feature extraction and increases the number of samples per subject, which benefits both model training and post-training majority voting. Each segmented sample is assigned a sampling rate label r for subsequent use. **6) Z-Score Normalization:** Z-score normalization is applied to each segmented sample, computed independently for each channel.

F.3. Detailed Per-Dataset Preprocessing

This section provides a basic description of raw data and detailed data preprocessing steps for each dataset.

AD-Auditory. The AD-Auditory (40Hz Auditory Entrainment) is a publicly available EEG dataset on the OpenNEURO website¹ from the paper (Lahijanian et al., 2024). It contains 35 subjects, including 17 AD, 6 MCI, 10 healthy controls, and 2 unknown subjects. This dataset aims to investigate the effect of entrainment on brain oscillations using EEG signal recordings during auditory brain stimulation for distinguish Alzheimer’s Disease. All the data are recorded using 19 monopolar channels (Fp1, Fp2, F7, F3, Fz, F4, F8, T3, C3, Cz, C4, T4, T5, P3, Pz, P4, T6, O1, and O2) based on the standard 10/20 system, with a sampling rate set to 250Hz. The dataset’s authors preprocess the data using the EEGLab toolbox in Matlab, which includes bandpass filtering, noise removal, artifact removal, re-referencing, and interpolating rejected channels, as described in their paper and on the data website. To maintain consistency with our pipeline, we perform additional preprocessing using the unified steps.

ADFSU. This is a publicly available dataset provided by Dr. Dennis Duke of Florida State University (Vicchiotti et al., 2023), which we refer to as ADFSU². It contains data from 80 AD subjects and 12 healthy subjects. Each

subject has a recording with a sampling frequency of 128Hz and an 8-second trial collected across 19 standard channels (Fp1, Fp2, F7, F3, Fz, F4, F8, T3, C3, Cz, C4, T4, T5, P3, Pz, P4, T6, O1, and O2) during both eye-open and eye-closed resting-state conditions. The preprocessing steps include band-pass filtering between 0.5 and 30 Hz, and an experienced EEG expert removes artifacts caused by movement. The data files are organized into "AD" and "Healthy" folders, with each folder containing "Eyes_open" and "Eyes_closed" subfolders to indicate the different tasks. Each task folder contains subject folders labeled with ID numbers, and all the data are stored in channel_name.txt files. Note that the eye-open data for the healthy subject with ID 5 is empty. For simplicity, we manually copy the eyes-closed data for this subject and use it as the eye-open data, avoiding handling empty files in the code. All subsequent preprocessing steps followed the same pipeline, without band-pass filtering or artifact removal.

ADFTD. The ADFTD-RS (A dataset of EEG recordings from Alzheimer’s disease, Frontotemporal dementia and Healthy subjects) is a publicly available resting-state EEG dataset on the OpenNEURO website³ from the paper (Miltiadous et al., 2023b;a), and a complementary dataset ADFTD-PS (A complementary dataset of open-eyes EEG recordings in a photo-stimulation setting from: Alzheimer’s disease, Frontotemporal dementia and Healthy subjects) in a photo-stimulation setting with exactly matched subjects⁴. It contains 88 subjects, including 36 AD, 23 Frontotemporal Dementia (FTD), and 29 healthy controls. For recording, a Nihon Kohden EEG 2100 clinical device is used, with 19 scalp electrodes (Fp1, Fp2, F7, F3, Fz, F4, F8, T3, C3, Cz, C4, T4, T5, P3, Pz, P4, T6, O1, and O2) according to the 10-20 international system and 2 reference electrodes (A1 and A2) placed on the mastoids for impedance check, according to the manual of the device. Each recording is performed according to the clinical protocol, with participants sitting with their eyes closed or in a photo-stimulation setting. The collection sampling rate is 500Hz. The dataset’s authors preprocess the data using the EEGLab toolbox in Matlab, which includes bandpass filtering, noise removal, artifact removal, re-referencing, and interpolating rejected channels, as described in their paper and on the data website. Since their preprocessing pipeline is already comprehensive, we only perform additional steps to align with our unified pipeline: downsampling to 200 Hz, applying multi-sampling segmentation, and Z-score normalization. Finally, we concatenated ADFTD-RS and ADFTD-PS into a single dataset (ADFTD) based on subject IDs.

¹<https://openneuro.org/datasets/ds005048/versions/1.0.0>

²<https://osf.io/2v5md/>

³<https://openneuro.org/datasets/ds004504/versions/1.0.8>

⁴<https://openneuro.org/datasets/ds006036/versions/1.0.5>

ADSZ. The ADSZ (Alzheimer’s Disease and Schizophrenia) dataset is a public EEG dataset⁵ from the paper (Alves et al., 2022). We use only the sub-dataset for Alzheimer’s disease (AD) available in the download link. This dataset contains data from 48 subjects, including 24 AD subjects and 24 healthy elderly subjects. The data are collected from 19 standard channels (Fp1, Fp2, F7, F3, Fz, F4, F8, T3, C3, Cz, C4, T4, T5, P3, Pz, P4, T6, O1, and O2) during eyes-open and eyes-closed resting states, with a sampling frequency of 128Hz. Most subjects have an EEG recording duration of 8 seconds, with minor 10, 12, or 14-second trials. The signals are preprocessed with band-pass filtering between 1-30 Hz, and an experienced EEG technician removes artifacts caused by subject movement. We use the same unified preprocessing pipeline described previously, without band-pass filtering or artifact removal.

APAVA. The APAVA (Alzheimer’s Patients’ Relatives Association of Valladolid) dataset⁶, referenced in the study by (Escudero et al., 2006), is a publicly available EEG dataset consisting of 23 subjects, including 12 AD subjects and 11 healthy elderly subjects. The data are recorded using 16 channels (Fp1, Fp2, F7, F3, F4, F8, T3, C3, C4, T4, T5, P3, P4, T6, O1, and O2) with a sampling frequency of 256Hz. Each subject has multiple trials, each lasting 5 seconds, yielding 1,280 timestamps. A specialist physician visually inspects the recordings to select data with minimal movement, electromyographic activity, or electrooculographic artifacts. We use the same unified preprocessing pipeline described previously, without band-pass filtering or artifact removal. As this dataset has a pre-defined data split, we do not use subject-independent cross-validation. We keep the same data split as in previous work (Wang et al., 2024b), where subject IDs 15, 16, 19, and 20 are in the validation set, IDs 1, 2, 17, and 18 are in the test set, and the remaining 15 subjects are in the training set.

BrainLat. The BrainLat⁷ (Latin American Brain Health Institute) dataset comprises multimodal neuroimaging data from 780 participants from Latin America (Prado et al., 2023). It contains two modalities: EEG and MRI. It includes five classes of subjects: Alzheimer’s disease (AD), behavioral variant frontotemporal dementia (bvFTD), multiple sclerosis (MS), Parkinson’s disease (PD), and healthy controls (HC). For EEG data recording, subjects are recorded in an eye-closed resting state inside a dimly lit, sound-attenuated, and electromagnetically shielded EEG room. They are instructed to remain still and awake, with a 128-channel Biosemi Active-Two acquisition system (pin-type,

active, sintered Ag-AgCl electrodes). The data are band-pass filtered between 0.5 and 40 Hz using a zero-phase shift Butterworth filter of order 8. The data are then down-sampled to 512 Hz, and Independent Component Analysis (ICA) is used to correct EEG artifacts induced by blinking and eye movements. We perform secondary preprocessing to match the pipeline of our method. EEG data for each subject are stored in folders labeled AR and CL, representing the subjects’ countries: Argentina and Chile. It is important to note that some subjects cannot read for unknown reasons, such as the subject named "sub-100013" (at least when we downloaded the dataset, which the data version was last modified by Dr. Pavel Prado on 7/2/2024). Additionally, not all subjects have EEG data; most subjects only have MRI datasets. In total, there are 135 functional subjects with EEG data across all five classes. Recordings were acquired using a BioSemi 128-channel system, which differs substantially from the standard 10-20 montage in electrode naming and placement. To ensure consistency across datasets, we performed channel alignment with the MNE-Python toolbox (Gramfort et al., 2013), mapping the 128 BioSemi electrodes to the 19 standard 10-20 channels using their 3D coordinates. All subsequent preprocessing steps followed the same pipeline.

CNBPM. The CNBPM is a large private EEG dataset provided by the AI-LAB laboratory at the University Mediteranea of Reggio Calabria, Italy, referenced in studies (Ieracitano et al., 2019b; Amezquita-Sanchez et al., 2019). It consists of 63 subjects with Alzheimer’s Disease (AD), 63 with Mild Cognitive Impairment (MCI), and 63 Healthy Control (HC) subjects. The data are collected using 19 standard channels (Fp1, Fp2, F7, F3, Fz, F4, F8, T3, C3, Cz, C4, T4, T5, P3, Pz, P4, T6, O1, and O2) with an initial sampling rate of 1024Hz. A frequency-band filter is applied to filter the frequency bands between 0.5 and 32 Hz, followed by downsampling to reduce the sampling rate to 256Hz. Visible blinks affected by artifacts are visually inspected and removed by an EEG expert. Since their preprocessing pipeline is already comprehensive, we only perform additional steps to align with our unified pipeline: downsampling to 200 Hz, applying multi-sampling segmentation, and Z-score normalization.

P-ADIC. The P-ADIC dataset, introduced in (Shor et al., 2021) and publicly available via DRYAD⁸, includes EEG recordings from 249 subjects (although the original paper reports 230). The dataset includes 49 individuals with Alzheimer’s Disease (AD), 34 with Mild Cognitive Impairment (MCI), 96 Healthy Controls (HC), 42 with Schizophrenia, and 28 with Depression. EEG signals are recorded using 19 standard channels (Fp1, Fp2, F7, F3, Fz, F4, F8,

⁵https://figshare.com/articles/dataset/Alzheimer_s_disease_and_Schizophrenia/19091771?file=33928037

⁶<https://osf.io/jbysn/>

⁷<https://www.synapse.org/Synapse:syn51549340/wiki/624187>

⁸<https://datadryad.org/dataset/doi:10.5061/dryad.8gtht76pw>

T3, C3, Cz, C4, T4, T5, P3, Pz, P4, T6, O1, O2) at an initial sampling rate of 500 Hz. We use the same unified preprocessing pipeline described before.

CAUEEG. The CAUEEG dataset, introduced in (Kim et al., 2023), is available upon request and contains 1,379 EEG recordings from 1,155 subjects. It includes 459 recordings from healthy controls (HC), 417 from individuals with Mild Cognitive Impairment (MCI), 311 with dementia, and 192 with other conditions. EEG signals were recorded using 19 standard channels (Fp1, F3, C3, P3, O1, Fp2, F4, C4, P4, O2, F7, T3, T5, F8, T4, T6, Fz, Cz, Pz) at a sampling rate of 200 Hz and pre-filtered with a 0.5–70 Hz bandpass filter. Data collection includes resting-state, photic stimulation, and limited hyperventilation tasks. We apply additional preprocessing to align with our pipeline. In line with the protocol described in (Kim et al., 2023), we treat each EEG recording as an independent subject. This decision is motivated by reported label shifts across sessions (e.g., HC to MCI, MCI to AD), which suggest that different recordings from the same individual should be considered distinct entities. Since this dataset provides detailed event annotations, we perform artifact removal via segment rejection rather than applying ICLabel. Specifically, segments labeled with terms such as ‘artifact’, ‘blink’, ‘eye’, ‘noise’, ‘movement’, ‘chewing’, ‘talk’, and related descriptors are removed, together with a 1-second buffer before and after each annotated event. The other preprocessing steps are the same as described before.

BACA-RS. The BACA-RS (Resting-state EEG data before and after cognitive activity across the adult lifespan and a 5-year follow-up) dataset is a publicly available EEG dataset on the OpenNEURO website⁹, referenced in the paper (Getzmann et al., 2024). According to the paper’s description, this dataset consists of 64 channels based on the 10-20 system, with the FCz electrode as an online reference. It includes resting-state EEG recordings from 608 subjects aged between 20 and 70 years, along with follow-up measurements of 208 subjects approximately 5 years later, starting in 2021. The EEG data are recorded with eyes open and eyes closed before and after a 2-hour block of cognitive experimental tasks. The EEG data are recorded at a 1000Hz sampling rate and filtered online using a 250Hz low-pass filter. This dataset aims to study the aging of brain activity in a resting state and provide a normal distribution of healthy subjects’ resting-state EEG for comparison with clinically relevant disorders. Since the recording dates of two trials can be 5 year separated, we are concerned that shifts in neurological condition may occur, potentially violating the assumption of subject-level consistency in COMET (Wang et al., 2023). As a result, we use trial-level consistency in-

⁹<https://openneuro.org/datasets/ds005385/versions/1.0.2>

stead for this dataset and treat trial ID as the label to guide contrastive pre-training. Therefore, a total of 816 trials are used. The other preprocessing steps are the same as described before.

Depression. The Depression (EEG: Depression rest) dataset is a publicly available EEG dataset on the OpenNEURO website¹⁰ from the paper (Cavanagh et al., 2019; Cavanagh, 2021). It contains data from 122 college-age subjects with healthy and different degrees of depression. The EEG data are recorded in a resting state, with instructions for eyes open and eyes closed, triggering one-minute spans of either open or closed eyes. Each subject’s depression level is labeled based on their score on the Beck Depression Inventory (BDI). The raw data sampling frequency is 500Hz. We use the same unified preprocessing pipeline described before.

FEP-PCR. The FEP-PCR dataset (EEG: First Episode Psychosis vs. Control Resting Task 1 & Task 2) is a publicly available EEG dataset separate on two pages on the OpenNEURO website^{11,12} from the paper (Phalen et al., 2020). It contains a total of 143 healthy and First-Episode Psychosis (FEP) subjects, with EEGs recorded using a 60-channel, low-impedance 10-10 system cap. We use the same unified preprocessing pipeline described before.

MCEF-RS. The MCEF-RS dataset (EEG Resting-state Microstates Correlates of Executive Functions) is a publicly available EEG dataset on the OpenNEURO website¹³ from the paper (Chenot et al., 2024). This study aimed to specifically explore the relationship between intrinsic brain spatio-temporal dynamics and Executive Functions. To do so, resting-state EEG microstates were used to assess brain spatio-temporal dynamics in 140 healthy participants, while a comprehensive battery of nine cognitive function tasks was employed to evaluate their executive functions. We use the same unified preprocessing pipeline.

PD-RS. The PD-RS (Rest eyes open) dataset is a publicly available EEG dataset on the OpenNEURO website¹⁴, referenced in the paper (Singh et al., 2023). This dataset includes 149 subjects, with 100 Parkinson’s disease (PD) subjects and 49 Healthy controls (HC) subjects. According to the description in their paper, the EEG data is recorded with a 64-channel BrainVision cap in a resting state with their eyes open for two minutes. The sampling frequency is set to 500Hz, and a 0.1Hz high-pass filter is applied to the EEG recordings. The Fully Automated Statistical Thresholding

¹⁰<https://openneuro.org/datasets/ds003478/versions/1.1.0>

¹¹<https://openneuro.org/datasets/ds003944/versions/1.0.1>

¹²<https://openneuro.org/datasets/ds003947/versions/1.0.1>

¹³<https://openneuro.org/datasets/ds005305/versions/1.0.1>

¹⁴<https://openneuro.org/datasets/ds004584/versions/1.0.0>

for EEG artifact Rejection (FASTER) algorithm rejects the bad channels and trials with greater than ± 3 Z-scores on key metrics and the `pop_rejchan` function from EEGLAB. Bad channels are interpolated except the mid-frontal Cz channel, which is never interpolated. Eye blink artifacts are removed following ICA. We use the same unified preprocessing pipeline described before.

PEARL-Neuro. The PEARL-Neuro (A Polish Electroencephalography, Alzheimer’s Risk-genes, Lifestyle and Neuroimaging) dataset is a publicly available EEG dataset on the OpenNEURO website¹⁵, referenced in the paper (Dzianok & Kublik, 2024). The full dataset contains data from 192 self-reported healthy middle-aged (50-63) subjects, with a balanced female-to-male ratio. Of these, 79 subjects are publicly available, and the dataset includes two modalities: EEG and fMRI. Other information, such as blood tests, demographics, and other health conditions, are also provided. The dataset aims to identify genetic variations associated with brain anatomical and functional phenotype imaging genomics, which could be potential biomarkers for predicting the risk of developing neurological and psychiatric disorders. This could lead to earlier diagnoses, more targeted treatments, and improved patient outcomes. EEG data are recorded using Brain Products systems, including an actiChamp amplifier and high-density actiCAP electrode caps with 128 electrodes (Brain Products GmbH, Munich, Germany). The FCz electrode is used as an online reference, and the sampling rate is set to 1000Hz with a low-pass filter at 280Hz. The dataset includes three different tasks: the Sternberg memory task (Sternberg), the Multi-source interference task (MSIT), and resting-state (rest). We perform secondary preprocessing to match the pipeline of our method. We only take the resting-state trials from each subject and apply our unified preprocessing pipeline.

SRM-RS. The REEG-SRM (SRM Resting-state EEG) dataset is a publicly available EEG dataset on the OpenNEURO website¹⁶, referenced in the paper (Hatlestad-Hall et al., 2022). This dataset contains resting-state EEG extracted from the experimental paradigm used in the Stimulus-Selective Response Modulation (SRM) project at the Department of Psychology, University of Oslo, Norway. The EEG data are recorded using 64 electrodes with a BioSemi ActiveTwo system, following the positional scheme of the 10-10 system. The dataset includes 111 healthy control subjects, with some subjects having one trial and others having multiple trials. The sampling rate is set to 1024Hz. Preprocessing steps are applied to the raw data, including bad channel interpolation, artifact rejection, and bandpass filtering from 1Hz to 45Hz. We exclude two

subjects who cannot read, identified as "sub-029" and "sub-104." For the remaining 109 subjects, we perform the same unified preprocessing pipeline described before.

TDBrain. The TDBrain (Two Decades-Brainclinics Research Archive for Insights in Neurophysiology) dataset^{17,18}, referenced in the paper (Van Dijk et al., 2022), is a large permission-available EEG time series dataset recording brain activities of 1274 subjects with 33 channels. Researchers need to send requests to the authors by filling out the application forms to get access to this dataset. This dataset aims to research neurological or psychiatric dysfunction, such as Major Depressive Disorder (MDD), attention deficit hyperactivity disorder (ADHD), Subjective Memory Complaints (SMC), obsessive-compulsive disorder (OCD), Parkinson’s disease (PD), and many other brain disorders. The EEG data is recorded in resting-states in eye-open and eye-closed states. The sampling rate is 500Hz. Preprocessing steps are applied to the raw data, including artifact rejection, 50Hz notch-frequency removal, and bandpass filtering from 0.5Hz to 100Hz. Some subjects in this dataset have "REPLICATION" and "NaN" labels, which are intended for the researcher’s model validation and testing by contacting them, as described in their paper. We retain them as no label is required for self-supervised pre-training. The other preprocessing steps are the same as described before.

TUEP. The TUEP¹⁹ is one of the datasets in The Temple University Hospital EEG Corpus (TUEG), which is one of the world’s largest open-source EEG corpora (Obeid & Picone, 2016). Researchers can access this dataset by submitting a request via an application form to the authors. This dataset is a subset of TUEG and contains data from 100 subjects with epilepsy and 100 subjects without epilepsy, as determined by a certified neurologist. Each subject in this dataset may have one or more sessions, and each session may have multiple trials. Some trials differ in the number of channels and sampling rates, and have gaps in years of collection. To ensure consistency, we first select only trials that contain all the 19 standard channels: Fp1, Fp2, F7, F3, Fz, F4, F8, T3, C3, Cz, C4, T4, T5, P3, Pz, P4, T6, O1, and O2. Since the recording dates of different trials can be widely separated, sometimes by several years, we are concerned that shifts in neurological condition may occur, potentially violating the assumption of subject-level consistency in COMET (Wang et al., 2023). As a result, we use trial-level consistency instead for this dataset and treat trial ID as the label to guide contrastive pre-training. Therefore, a total of 2012 trials are used. All other preprocessing steps follow the same pipeline described previously.

¹⁵<https://openneuro.org/datasets/ds004796/versions/1.0.9>

¹⁶<https://openneuro.org/datasets/ds003775/versions/1.2.1>

¹⁷<https://brainclinics.com/resources/>

¹⁸<https://www.synapse.org/Synapse:syn25671079/wiki/610278>

¹⁹https://isip.piconepress.com/projects/nedc/html/tuh_eeeg/

G. Detailed Results

This section reports detailed experimental results for different tasks, including baseline method comparisons and per-subject analysis. The evaluation is conducted on five downstream datasets: ADFSU, ADFTD, ADSZ, APAVA, and CNBPM. We report all 14 evaluation metrics, including sample-level accuracy, precision (macro-averaged), sensitivity/recall (macro-averaged), specificity (macro-averaged), F1 score (macro-averaged), AUROC (macro-averaged), and AUPRC (macro-averaged), and their corresponding subject-level metrics computed via majority voting (See para. 2.2).

G.1. Method Comparison Results

The detailed results for baseline method comparisons on five downstream datasets are presented in Table 7 (ADFSU), Table 8 (ADFTD), Table 9 (ADSZ), Table 10 (APAVA), and Table 11 (CNBPM), respectively.

G.2. Per-Subject Analysis

The detailed results for the per-subject analysis under the leave-one-subject-out (LOSO) setting on the ADFTD dataset are presented in Table 12 and Table 13.

Table 7. Method Comparison Detailed Results on ADFSU. The detailed results comparison between our method and baseline methods on the dataset ADFSU includes all 7 evaluation metrics. The **Top-1**, **Top-2**, and **Top-3** results are highlighted in red, blue, and green.

Datasets	Models	Accuracy	Precision	Sensitivity	Specificity	F1 Score	AUROC	AUPRC	
ADFSU (Sample-Level) (4,048 Samples) (HC vs AD)	ManualFeature	87.40±3.88	82.55±9.01	73.87±10.80	73.87±10.80	75.67±11.41	80.90±8.87	77.35±9.05	
	EEGConformer	96.53±1.93	96.75±2.12	92.33±4.46	92.33±4.46	94.22±3.28	98.87±0.95	98.36±1.24	
	EEGInception	94.60±0.98	94.49±1.15	88.63±4.21	88.63±4.21	90.88±2.13	98.73±0.75	97.99±1.19	
	EEGNet	82.27±10.27	77.52±10.71	74.92±6.79	74.92±6.79	74.48±9.91	85.88±7.95	82.41±10.23	
	iTransformer	87.80±1.07	86.93±3.61	72.75±2.50	72.75±2.50	76.80±2.31	88.16±1.86	85.59±1.34	
	MedGNN	94.13±1.50	94.34±3.59	87.08±1.86	87.08±1.86	90.09±2.37	98.06±1.42	97.08±2.13	
	Medformer	92.73±0.80	93.58±0.78	83.33±2.71	83.33±2.71	87.15±1.91	97.48±1.32	96.30±1.18	
	MNet	88.40±3.38	90.34±3.43	72.12±8.24	72.12±8.24	76.19±8.72	92.75±5.08	90.30±5.71	
	ModernTCN	87.80±1.19	90.98±2.03	70.38±2.93	70.38±2.93	75.09±3.18	91.94±1.84	89.57±2.09	
	PatchTST	87.13±1.42	83.81±2.01	72.83±4.55	72.83±4.55	76.03±4.27	89.12±1.95	85.53±2.14	
	TCN	94.27±1.70	95.07±2.54	86.79±3.71	86.79±3.71	90.10±3.13	98.82±0.73	98.00±1.23	
	TimesNet	90.60±2.39	92.28±2.38	77.88±6.26	77.88±6.26	82.08±6.29	95.21±2.45	93.39±2.27	
	BIOT	93.47±1.51	92.80±2.71	86.17±2.83	86.17±2.83	88.94±2.69	96.78±3.04	95.60±3.05	
	LaBraM	95.47±1.77	96.14±0.98	89.67±4.97	89.67±4.97	92.24±3.38	98.90±0.53	97.98±0.88	
	CBraMod	95.40±2.28	94.56±2.40	90.88±5.60	90.88±5.60	92.32±4.27	98.47±1.49	97.59±2.27	
	CSBrain	94.67±1.14	93.96±1.28	89.17±3.69	89.17±3.69	91.11±2.34	98.23±0.51	97.23±0.63	
	LEAD (Ours)	98.18±0.61	98.70±0.44	95.62±1.54	95.62±1.54	97.06±1.02	99.92±0.07	99.85±0.13	
	ADFSU (Subject-Level) (92 Subjects) (HC vs AD)	ManualFeature	92.00±7.48	85.78±23.02	80.00±18.71	80.00±18.71	81.05±20.29	80.00±18.71	91.56±7.62
		EEGConformer	100.00±0.00	100.00±0.00	100.00±0.00	100.00±0.00	100.00±0.00	100.00±0.00	100.00±0.00
EEGInception		100.00±0.00	100.00±0.00	100.00±0.00	100.00±0.00	100.00±0.00	100.00±0.00	100.00±0.00	
EEGNet		88.00±11.66	80.89±23.26	81.25±18.54	81.25±18.54	78.37±21.07	81.25±18.54	92.28±7.50	
iTransformer		86.00±4.90	72.67±26.67	65.00±12.25	65.00±12.25	66.01±17.61	65.00±12.25	85.33±4.35	
MedGNN		100.00±0.00	100.00±0.00	100.00±0.00	100.00±0.00	100.00±0.00	100.00±0.00	100.00±0.00	
Medformer		100.00±0.00	100.00±0.00	100.00±0.00	100.00±0.00	100.00±0.00	100.00±0.00	100.00±0.00	
MNet		84.00±4.90	61.78±26.67	60.00±12.25	60.00±12.25	58.82±17.61	60.00±12.25	83.56±4.35	
ModernTCN		84.00±4.90	61.78±26.67	60.00±12.25	60.00±12.25	58.82±17.61	60.00±12.25	83.56±4.35	
PatchTST		90.00±6.32	84.67±22.44	75.00±15.81	75.00±15.81	77.12±18.02	75.00±15.81	89.33±6.35	
TCN		98.00±4.00	98.89±2.22	95.00±10.00	95.00±10.00	96.08±7.84	95.00±10.00	97.78±4.44	
TimesNet		94.00±8.00	86.89±23.54	85.00±20.00	85.00±20.00	84.97±21.64	85.00±20.00	93.78±8.12	
BIOT		100.00±0.00	100.00±0.00	100.00±0.00	100.00±0.00	100.00±0.00	100.00±0.00	100.00±0.00	
LaBraM		100.00±0.00	100.00±0.00	100.00±0.00	100.00±0.00	100.00±0.00	100.00±0.00	100.00±0.00	
CBraMod		100.00±0.00	100.00±0.00	100.00±0.00	100.00±0.00	100.00±0.00	100.00±0.00	100.00±0.00	
CSBrain		100.00±0.00	100.00±0.00	100.00±0.00	100.00±0.00	100.00±0.00	100.00±0.00	100.00±0.00	
LEAD (Ours)		100.00±0.00							

Table 8. Method Comparison Detailed Results on ADFTD. The detailed results comparison between our method and baseline methods on the dataset ADFTD includes all 7 evaluation metrics. The **Top-1**, **Top-2**, and **Top-3** results are highlighted in red, blue, and green.

Datasets	Models	Accuracy	Precision	Sensitivity	Specificity	F1 Score	AUROC	AUPRC	
ADFTD (Sample-Level) (167,083 Samples) (HC vs AD vs FTD)	ManualFeature	46.98±4.11	45.82±4.61	45.27±4.08	73.13±2.00	44.73±3.88	62.89±4.31	43.69±3.63	
	EEGConformer	61.28±2.83	62.39±4.23	58.82±3.53	79.87±1.51	58.59±3.84	80.61±3.90	69.14±5.37	
	EEGInception	64.25±3.85	66.62±2.85	64.03±3.63	82.16±1.76	62.69±4.06	84.01±2.76	73.69±2.34	
	EEGNet	45.22±3.93	40.83±8.66	42.91±4.03	71.60±1.93	40.31±6.74	60.93±4.42	43.59±5.12	
	iTransformer	56.27±3.61	54.65±3.95	54.71±3.55	77.93±1.73	54.33±3.67	73.98±4.02	59.26±5.30	
	MedGNN	69.60±3.85	70.22±4.07	68.15±4.74	84.48±2.16	67.67±4.60	85.52±2.57	76.86±3.18	
	Medformer	66.66±4.89	67.19±4.49	65.13±6.15	82.80±2.69	64.83±6.72	84.13±3.27	74.59±5.16	
	MNet	63.92±6.05	63.84±8.01	61.89±7.28	81.46±3.11	59.91±9.77	82.30±5.04	71.32±8.50	
	ModernTCN	60.38±3.42	59.21±3.91	58.59±3.67	79.82±1.71	58.52±3.71	77.25±3.33	63.44±4.55	
	PatchTST	55.48±3.23	54.35±6.92	52.24±2.94	76.72±1.53	50.95±4.04	71.30±4.75	56.53±6.94	
	TCN	66.04±2.46	64.89±2.47	64.44±2.31	82.68±1.19	64.26±2.40	82.94±1.89	71.43±3.32	
	TimesNet	61.85±3.37	61.12±4.68	59.71±4.92	80.38±1.87	58.66±5.68	79.18±3.39	66.48±6.35	
	BIOT	70.94±5.66	70.86±5.53	69.86±5.91	85.14±2.96	69.79±5.90	86.85±4.77	78.40±6.69	
	LaBraM	77.00±3.76	77.33±2.84	75.79±4.53	88.24±2.02	75.64±4.68	91.22±2.72	84.75±4.41	
	CBraMod	69.92±3.95	69.52±4.41	68.58±3.97	84.60±1.94	68.33±4.53	86.95±2.89	78.06±4.26	
	CSBrain	70.67±2.12	70.41±2.03	69.60±2.49	85.02±1.11	69.39±2.63	86.82±1.28	78.66±1.93	
	LEAD (Ours)	81.70±4.74	82.93±4.40	80.78±4.95	90.52±2.45	81.01±5.02	94.03±1.33	90.37±2.14	
	ADFTD (Subject-Level) (88 Subjects) (HC vs AD vs FTD)	ManualFeature	62.00±4.00	56.03±15.90	59.44±4.16	80.16±1.81	54.26±7.80	69.80±2.94	53.37±4.75
		EEGConformer	74.00±10.20	70.95±20.86	72.22±10.97	86.03±5.35	68.45±15.21	79.13±8.16	66.26±12.37
EEGInception		82.00±13.27	80.67±21.12	81.67±13.68	90.79±6.78	79.47±17.70	86.23±10.23	76.08±17.02	
EEGNet		64.00±10.20	58.81±22.32	60.56±11.17	80.63±5.60	54.82±14.34	70.60±8.38	54.25±10.70	
iTransformer		72.00±7.48	72.56±14.91	70.56±7.16	85.87±3.56	67.17±9.15	78.21±5.36	61.84±6.73	
MedGNN		78.00±4.00	83.33±2.79	77.78±4.65	89.05±2.09	75.23±4.81	83.41±3.30	69.28±4.90	
Medformer		80.00±10.95	84.11±8.15	80.00±11.17	89.68±5.66	78.98±12.08	84.84±8.41	73.44±14.44	
MNet		74.00±12.00	70.30±21.93	73.33±13.10	86.83±5.89	68.63±17.53	80.08±9.49	66.72±14.24	
ModernTCN		78.00±7.48	78.37±13.91	77.22±8.85	88.41±4.16	74.39±11.35	82.82±6.50	71.16±9.55	
PatchTST		72.00±9.80	68.81±21.28	69.44±10.24	85.08±5.00	65.04±14.32	77.26±7.62	62.33±12.48	
TCN		84.00±4.90	88.67±4.40	83.33±5.83	91.43±2.81	82.80±6.10	87.38±4.32	78.49±6.23	
TimesNet		72.00±11.66	61.86±21.27	71.11±13.10	86.03±5.82	64.23±17.73	78.57±9.45	63.38±14.25	
BIOT		88.00±9.80	91.11±7.54	87.78±10.03	93.65±5.19	88.10±9.72	90.71±7.61	83.72±13.29	
LaBraM		92.00±7.48	94.44±4.65	91.67±8.24	95.87±4.09	91.14±8.64	93.77±6.16	88.78±10.19	
CBraMod		84.00±4.90	88.78±4.13	82.78±5.09	91.43±2.48	82.21±6.30	87.10±3.77	77.31±6.86	
CSBrain		80.00±6.32	84.67±4.88	79.44±6.24	89.68±3.01	78.33±7.52	84.56±4.61	72.03±8.23	
LEAD (Ours)		94.00±4.90	95.67±3.59	93.89±5.09	96.83±2.61	93.95±4.95	95.36±3.85	91.56±6.91	

Table 9. Method Comparison Detailed Results on ADSZ. The detailed results comparison between our method and baseline methods on the dataset ADSZ includes all 7 evaluation metrics. The **Top-1**, **Top-2**, and **Top-3** results are highlighted in red, blue, and green.

Datasets	Models	Accuracy	Precision	Sensitivity	Specificity	F1 Score	AUROC	AUPRC	
ADSZ (Sample-Level) (1,128 Samples) (HC vs AD)	ManualFeature	65.64±13.56	55.33±25.09	64.85±14.35	64.85±14.35	58.42±21.26	67.20±15.34	64.07±12.94	
	EEGConformer	94.73±3.47	94.91±3.36	94.91±3.32	94.91±3.32	94.73±3.47	98.50±1.48	98.52±1.49	
	EEGInception	92.62±4.43	93.43±3.85	92.93±4.16	92.93±4.16	92.60±4.44	98.06±1.66	98.04±1.75	
	EEGNet	66.27±12.39	71.26±13.28	67.19±12.37	67.19±12.37	64.90±12.88	77.18±19.10	78.29±17.21	
	iTransformer	73.29±4.86	73.91±5.53	73.30±4.80	73.30±4.80	73.13±4.75	81.86±4.90	82.02±5.15	
	MedGNN	88.62±8.00	89.11±7.79	88.84±7.86	88.84±7.86	88.59±8.01	95.90±4.10	96.05±3.98	
	Medformer	88.78±5.71	88.81±5.76	88.73±5.77	88.73±5.77	88.73±5.76	94.18±3.72	94.22±3.91	
	MNet	79.26±7.34	79.67±7.36	79.42±7.29	79.42±7.29	79.21±7.35	88.87±5.92	89.64±5.23	
	ModernTCN	76.15±3.85	77.15±3.25	75.94±3.83	75.94±3.83	75.73±4.05	84.42±4.30	84.40±4.18	
	PatchTST	71.13±10.02	71.93±10.56	71.48±10.34	71.48±10.34	71.05±10.02	79.10±12.54	79.27±11.47	
	TCN	89.00±9.14	89.05±9.28	88.93±9.25	88.93±9.25	88.93±9.23	94.02±6.85	93.44±7.78	
	TimesNet	83.88±3.58	84.16±3.47	83.87±3.57	83.87±3.57	83.80±3.60	88.12±9.12	87.78±9.75	
	BIOT	90.88±4.66	91.44±4.13	91.04±4.75	91.04±4.75	90.83±4.72	96.73±2.98	96.52±3.55	
	LaBraM	91.23±4.37	92.10±3.37	91.16±4.38	91.16±4.38	91.12±4.50	97.54±1.88	97.58±1.94	
	CBraMod	84.46±8.37	88.51±4.55	84.62±8.54	84.62±8.54	83.70±9.28	96.67±3.69	96.77±3.44	
	CSBrain	93.18±4.03	93.66±3.56	93.36±3.78	93.36±3.78	93.16±4.03	98.87±1.14	98.92±1.10	
	LEAD (Ours)	97.42±2.74	97.60±2.59	97.51±2.57	97.51±2.57	97.42±2.74	100.00±0.00	100.00±0.00	
	ADSZ (Subject-Level) (48 Subjects) (HC vs AD)	ManualFeature	70.00±24.49	60.00±33.91	70.00±24.49	70.00±24.49	63.05±30.68	70.00±24.49	70.00±24.49
		EEGConformer	100.00±0.00	100.00±0.00	100.00±0.00	100.00±0.00	100.00±0.00	100.00±0.00	100.00±0.00
EEGInception		100.00±0.00	100.00±0.00	100.00±0.00	100.00±0.00	100.00±0.00	100.00±0.00	100.00±0.00	
EEGNet		66.67±18.26	67.00±26.38	66.67±18.26	66.67±18.26	61.38±22.11	66.67±18.26	65.33±18.45	
iTransformer		100.00±0.00	100.00±0.00	100.00±0.00	100.00±0.00	100.00±0.00	100.00±0.00	100.00±0.00	
MedGNN		96.67±6.67	97.50±5.00	96.67±6.67	96.67±6.67	96.57±6.86	96.67±6.67	96.67±6.67	
Medformer		100.00±0.00	100.00±0.00	100.00±0.00	100.00±0.00	100.00±0.00	100.00±0.00	100.00±0.00	
MNet		90.00±13.33	90.83±13.02	90.00±13.33	90.00±13.33	89.90±13.38	90.00±13.33	87.22±16.25	
ModernTCN		90.00±8.16	92.50±6.12	90.00±8.16	90.00±8.16	89.71±8.40	90.00±8.16	85.00±12.25	
PatchTST		86.67±19.44	87.50±19.36	86.67±19.44	86.67±19.44	86.29±19.99	86.67±19.44	86.67±19.44	
TCN		96.67±6.67	97.50±5.00	96.67±6.67	96.67±6.67	96.57±6.86	96.67±6.67	95.00±10.00	
TimesNet		96.67±6.67	97.50±5.00	96.67±6.67	96.67±6.67	96.57±6.86	96.67±6.67	95.00±10.00	
BIOT		90.88±4.66	91.44±4.13	91.04±4.75	91.04±4.75	90.83±4.72	96.73±2.98	96.52±3.55	
LaBraM		100.00±0.00	100.00±0.00	100.00±0.00	100.00±0.00	100.00±0.00	100.00±0.00	100.00±0.00	
CBraMod		90.00±13.33	93.50±8.31	90.00±13.33	90.00±13.33	89.07±14.85	90.00±13.33	87.00±16.61	
CSBrain		100.00±0.00	100.00±0.00	100.00±0.00	100.00±0.00	100.00±0.00	100.00±0.00	100.00±0.00	
LEAD (Ours)		100.00±0.00	100.00±0.00	100.00±0.00	100.00±0.00	100.00±0.00	100.00±0.00	100.00±0.00	

Table 10. Method Comparison Detailed Results on APAVA. The detailed results comparison between our method and baseline methods on the dataset APAVA includes all 7 evaluation metrics. The **Top-1**, **Top-2**, and **Top-3** results are highlighted in red, blue, and green.

Datasets	Models	Accuracy	Precision	Sensitivity	Specificity	F1 Score	AUROC	AUPRC
APAVA <i>(Sample-Level)</i> <i>(9,282 Samples)</i> <i>(HC vs AD)</i>	ManualFeature	70.40±4.92	77.53±8.45	64.55±5.25	64.55±5.25	63.22±6.51	66.49±5.78	64.17±5.79
	EEGConformer	76.90±3.19	81.85±2.78	72.65±4.10	72.65±4.10	73.05±4.93	83.07±3.70	83.43±3.70
	EEGInception	71.38±2.38	72.95±2.80	68.11±3.64	68.11±3.64	67.84±4.60	78.04±4.19	78.65±3.34
	EEGNet	71.38±2.38	72.95±2.80	68.11±3.64	68.11±3.64	67.84±4.60	78.04±4.19	78.65±3.34
	iTransformer	74.51±1.52	74.88±1.21	71.67±2.24	71.67±2.24	72.13±2.30	85.53±1.00	83.37±1.39
	MedGNN	73.71±4.64	81.38±2.00	68.40±5.99	68.40±5.99	67.54±7.95	81.39±3.83	82.69±3.50
	Medformer	71.99±1.67	74.97±2.64	67.47±2.03	67.47±2.03	67.42±2.44	78.38±2.75	78.33±2.96
	MNet	65.87±4.04	79.55±1.05	58.52±5.31	58.52±5.31	52.98±8.72	79.85±3.17	80.30±3.26
	ModernTCN	67.24±0.54	73.27±2.32	60.87±0.54	60.87±0.54	58.42±0.76	75.88±2.41	76.25±2.12
	PatchTST	64.54±0.37	75.24±6.16	57.34±0.79	57.34±0.79	52.39±2.65	73.76±3.11	72.85±3.27
	TCN	78.16±3.07	82.81±2.51	74.26±4.16	74.26±4.16	74.81±4.47	85.84±3.92	86.33±3.81
	TimesNet	66.71±3.77	74.47±6.25	59.80±4.51	59.80±4.51	55.95±6.89	56.01±4.93	59.13±5.35
	BIOT	81.62±3.83	84.08±2.35	78.92±5.17	78.92±5.17	79.55±5.36	92.92±2.77	92.33±2.89
	LaBraM	74.24±1.74	75.28±1.25	71.52±3.22	71.52±3.22	71.65±3.35	85.61±1.20	83.91±1.44
	CBraMod	75.51±3.19	76.27±4.83	73.93±1.74	73.93±1.74	74.10±2.40	83.10±1.85	82.97±2.10
	CSBrain	70.16±5.00	78.21±4.83	63.95±6.04	63.95±6.04	61.69±8.63	68.20±1.53	68.80±2.51
	LEAD (Ours)	84.36±5.33	84.41±5.72	83.36±4.91	83.36±4.91	83.70±5.30	92.51±4.33	92.23±4.80
APAVA <i>(Subject-Level)</i> <i>(23 Subjects)</i> <i>(HC vs AD)</i>	ManualFeature	65.00±12.25	60.00±28.58	65.00±12.25	65.00±12.25	57.33±19.60	65.00±12.25	60.00±8.16
	EEGConformer	70.00±10.00	71.67±23.33	70.00±10.00	70.00±10.00	65.33±16.00	70.00±10.00	63.33±6.67
	EEGInception	75.00±15.81	75.00±25.82	75.00±15.81	75.00±15.81	70.67±21.33	75.00±15.81	70.00±16.33
	EEGNet	75.00±15.81	75.00±25.82	75.00±15.81	75.00±15.81	70.67±21.33	75.00±15.81	70.00±16.33
	iTransformer	85.00±12.25	90.00±8.16	85.00±12.25	85.00±12.25	84.00±13.06	85.00±12.25	80.00±16.33
	MedGNN	70.00±10.00	71.67±23.33	70.00±10.00	70.00±10.00	65.33±16.00	70.00±10.00	63.33±6.67
	Medformer	75.00±0.00	83.33±0.00	75.00±0.00	75.00±0.00	73.33±0.00	75.00±0.00	66.67±0.00
	MNet	55.00±10.00	36.67±23.33	55.00±10.00	55.00±10.00	41.33±16.00	55.00±10.00	53.33±6.67
	ModernTCN	50.00±0.00	25.00±0.00	50.00±0.00	50.00±0.00	33.33±0.00	50.00±0.00	50.00±0.00
	PatchTST	50.00±0.00	25.00±0.00	50.00±0.00	50.00±0.00	33.33±0.00	50.00±0.00	50.00±0.00
	TCN	75.00±0.00	83.33±0.00	75.00±0.00	75.00±0.00	73.33±0.00	75.00±0.00	66.67±0.00
	TimesNet	50.00±0.00	25.00±0.00	50.00±0.00	50.00±0.00	33.33±0.00	50.00±0.00	50.00±0.00
	BIOT	95.00±10.00	96.67±6.67	95.00±10.00	95.00±10.00	94.67±10.67	95.00±10.00	93.33±13.33
	LaBraM	75.00±15.81	75.00±25.82	75.00±15.81	75.00±15.81	70.67±21.33	75.00±15.81	70.00±16.33
	CBraMod	75.00±0.00	83.33±0.00	75.00±0.00	75.00±0.00	73.33±0.00	75.00±0.00	68.33±3.33
	CSBrain	65.00±12.25	60.00±28.58	65.00±12.25	65.00±12.25	57.33±19.60	65.00±12.25	60.00±8.16
	LEAD (Ours)	100.00±0.00						

Table 11. Method Comparison Detailed Results on CNBPM. The detailed results comparison between ours and baseline methods on the dataset CNBPM includes all 7 evaluation metrics. The **Top-1**, **Top-2**, and **Top-3** results are highlighted in red, blue, and green.

Datasets	Models	Accuracy	Precision	Sensitivity	Specificity	F1 Score	AUROC	AUPRC
CNBPM (Sample-Level) (122,029 Samples) (HC vs MCI vs AD)	ManualFeature	48.25±8.11	44.08±6.56	43.80±6.72	73.56±3.95	43.00±6.36	61.29±6.44	41.05±5.17
	EEGConformer	65.30±11.18	59.85±8.02	59.20±9.36	82.13±5.87	59.17±8.85	81.76±8.20	64.85±9.17
	EEGInception	63.46±10.08	59.60±8.14	60.67±7.85	82.05±4.86	58.56±8.02	81.73±8.18	63.95±8.58
	EEGNet	47.94±7.22	44.16±5.91	41.54±6.09	72.20±3.97	38.57±6.52	63.51±7.95	45.73±5.71
	iTransformer	59.25±11.23	52.26±7.65	51.91±7.86	78.98±5.65	51.37±8.01	74.99±10.16	56.17±8.73
	MedGNN	65.34±9.04	59.36±7.76	59.06±7.98	81.88±4.88	58.68±7.50	82.13±7.35	65.80±7.03
	Medformer	66.31±10.00	61.15±8.05	60.75±8.15	82.55±5.20	60.39±7.68	82.17±7.87	66.25±7.41
	MNet	61.43±13.81	55.07±11.03	50.29±9.33	78.82±6.67	47.04±9.76	77.03±11.79	58.95±10.49
	ModernTCN	61.45±10.53	57.87±7.74	56.64±7.91	80.86±5.12	55.94±8.10	77.85±9.30	59.69±9.22
	PatchTST	57.43±9.39	51.20±6.10	50.79±5.75	77.75±4.22	49.78±6.10	71.52±9.58	53.69±8.24
	TCN	66.04±7.33	58.90±5.09	59.22±4.67	82.65±3.92	58.71±5.02	82.01±6.02	63.40±5.42
	TimesNet	63.56±10.91	57.30±7.40	56.12±6.36	81.31±5.29	56.19±6.63	79.18±7.74	60.17±7.70
	BIOT	61.70±13.03	55.70±9.53	54.96±9.21	80.37±6.36	54.79±9.52	77.95±11.46	59.39±11.05
	LaBraM	61.01±12.20	53.32±7.36	53.59±6.21	79.88±6.05	52.66±7.11	78.44±9.59	59.05±8.20
	CBraMod	61.84±10.71	54.79±7.13	54.14±6.75	79.78±5.67	53.93±6.87	78.68±9.10	60.68±7.13
	CSBrain	67.11±7.61	60.96±5.77	60.59±4.80	82.69±3.85	60.30±5.41	83.39±5.73	66.55±5.21
LEAD (Ours)	66.00±11.35	62.51±7.23	59.73±6.56	81.41±5.82	60.20±6.83	79.10±10.21	65.59±9.75	
CNBPM (Subject-Level) (189 Subjects) (HC vs MCI vs AD)	ManualFeature	48.57±5.55	42.29±10.06	48.57±5.55	74.29±2.78	43.95±7.64	61.43±4.16	42.09±3.50
	EEGConformer	60.00±7.74	68.74±8.17	60.00±7.74	80.00±3.87	58.42±8.60	70.00±5.80	53.18±6.41
	EEGInception	60.95±7.62	61.35±9.41	60.95±7.62	80.48±3.81	59.77±8.06	70.71±5.71	53.16±6.39
	EEGNet	40.00±9.81	35.17±17.28	40.00±9.81	70.00±4.90	34.02±11.43	55.00±7.35	38.50±5.60
	iTransformer	56.19±7.00	57.95±9.63	56.19±7.00	78.10±3.50	52.85±8.58	67.14±5.25	49.03±5.92
	MedGNN	54.29±10.26	56.81±15.83	54.29±10.26	77.14±5.13	52.18±11.32	65.71±7.69	48.00±6.90
	Medformer	62.86±5.55	64.22±7.00	62.86±5.55	81.43±2.78	60.93±6.49	72.14±4.16	54.28±4.42
	MNet	49.52±5.71	34.50±3.91	49.52±5.71	74.76±2.86	39.97±4.38	62.14±4.29	42.79±3.51
	ModernTCN	63.81±7.13	66.42±10.20	63.81±7.13	81.90±3.56	61.96±9.90	72.86±5.35	56.23±5.39
	PatchTST	56.19±5.55	56.83±16.05	56.19±5.55	78.10±2.78	51.35±9.07	67.14±4.16	49.16±5.15
	TCN	63.81±3.81	63.66±3.19	63.81±3.81	81.90±1.90	62.66±3.41	72.86±2.86	54.45±3.21
	TimesNet	57.14±5.22	59.11±9.17	57.14±5.22	78.57±2.61	55.52±4.93	67.86±3.91	50.34±4.43
	BIOT	57.14±7.97	58.87±8.30	57.14±7.97	78.57±3.98	55.74±8.58	67.86±5.98	49.21±6.42
	LaBraM	53.33±4.67	50.22±7.99	53.33±4.67	76.67±2.33	50.11±6.53	65.00±3.50	45.76±3.58
	CBraMod	54.29±9.33	52.97±13.37	54.29±9.33	77.14±4.67	50.60±10.89	65.71±7.00	47.90±6.64
	CSBrain	63.81±4.86	64.93±7.29	63.81±4.86	81.90±2.43	62.41±5.80	72.86±3.64	54.65±4.85
LEAD (Ours)	66.67±6.73	70.08±8.94	66.67±6.73	83.33±3.37	65.94±6.66	75.00±5.05	57.90±6.69	

Table 12. First Part of per-subject results of ADFTD. Demographic information, MMSE, recording length, and per-subject results using the LOSO setting of all subjects from Sub-001 to Sub-065.

Subject ID	Gender	Age	Class	MMSE	Length	Sample-level Accuracy	Subject-level Accuracy
Sub-001	F	57	AD	16	0.25h	77.13%	✓
Sub-002	F	78	AD	22	0.33h	40.35%	✗
Sub-003	M	70	AD	14	0.16h	82.44%	✓
Sub-004	F	67	AD	20	0.29h	95.04%	✓
Sub-005	M	70	AD	22	0.30h	96.08%	✓
Sub-006	F	61	AD	14	0.28h	58.93%	✓
Sub-007	F	79	AD	20	0.33h	92.98%	✓
Sub-008	M	62	AD	16	0.33h	79.14%	✓
Sub-009	F	77	AD	23	0.28h	73.26%	✓
Sub-010	M	69	AD	20	0.44h	54.76%	✓
Sub-011	M	71	AD	22	0.29h	89.66%	✓
Sub-012	M	63	AD	18	0.34h	74.04%	✓
Sub-013	F	64	AD	20	0.36h	92.89%	✓
Sub-014	M	77	AD	14	0.40h	85.86%	✓
Sub-015	M	61	AD	18	0.33h	87.08%	✓
Sub-016	F	68	AD	14	0.39h	94.99%	✓
Sub-017	F	61	AD	6	0.35h	98.31%	✓
Sub-018	F	73	AD	23	0.34h	98.53%	✓
Sub-019	F	62	AD	14	0.34h	59.57%	✓
Sub-020	M	71	AD	4	0.35h	94.01%	✓
Sub-021	M	79	AD	22	0.30h	79.66%	✓
Sub-022	F	68	AD	20	0.30h	94.78%	✓
Sub-023	M	60	AD	16	0.25h	69.73%	✓
Sub-024	F	69	AD	20	0.23h	98.96%	✓
Sub-025	F	79	AD	20	0.26h	31.06%	✗
Sub-026	F	61	AD	18	0.27h	97.96%	✓
Sub-027	F	67	AD	16	0.26h	99.50%	✓
Sub-028	M	49	AD	20	0.33h	91.12%	✓
Sub-029	F	53	AD	16	0.23h	96.75%	✓
Sub-030	F	56	AD	20	0.18h	99.47%	✓
Sub-031	F	67	AD	22	0.34h	75.28%	✓
Sub-032	F	59	AD	20	0.24h	85.07%	✓
Sub-033	F	72	AD	20	0.22h	70.55%	✓
Sub-034	F	75	AD	18	0.29h	93.91%	✓
Sub-035	F	57	AD	22	0.32h	91.30%	✓
Sub-036	F	58	AD	9	0.26h	62.05%	✓
Sub-037	M	57	HC	30	0.37h	75.66%	✓
Sub-038	M	62	HC	30	0.35h	93.12%	✓
Sub-039	M	70	HC	30	0.34h	88.15%	✓
Sub-040	M	61	HC	30	0.32h	80.61%	✓
Sub-041	F	77	HC	30	0.34h	81.21%	✓
Sub-042	M	74	HC	30	0.33h	91.37%	✓
Sub-043	M	72	HC	30	0.31h	92.28%	✓
Sub-044	F	64	HC	30	0.38h	87.45%	✓
Sub-045	F	70	HC	30	0.34h	77.45%	✓
Sub-046	M	63	HC	30	0.36h	85.24%	✓
Sub-047	F	70	HC	30	0.34h	90.48%	✓
Sub-048	M	65	HC	30	0.38h	88.31%	✓
Sub-049	F	62	HC	30	0.34h	76.68%	✓
Sub-050	M	68	HC	30	0.31h	96.14%	✓
Sub-051	F	75	HC	30	0.33h	94.02%	✓
Sub-052	F	73	HC	30	0.33h	74.64%	✓
Sub-053	M	70	HC	30	0.31h	94.20%	✓
Sub-054	M	78	HC	30	0.35h	92.48%	✓
Sub-055	M	67	HC	30	0.33h	82.26%	✓
Sub-056	F	64	HC	30	0.34h	81.32%	✓
Sub-057	M	64	HC	30	0.32h	92.14%	✓
Sub-058	M	62	HC	30	0.27h	77.62%	✓
Sub-059	M	77	HC	30	0.30h	67.08%	✓
Sub-060	F	71	HC	30	0.33h	95.32%	✓
Sub-061	F	63	HC	30	0.33h	77.05%	✓
Sub-062	M	67	HC	30	0.35h	51.18%	✓
Sub-063	M	66	HC	30	0.34h	84.08%	✓
Sub-064	M	66	HC	30	0.35h	97.25%	✓
Sub-065	F	71	HC	30	0.30h	93.43%	✓

Table 13. Second Part of per-subject results of ADFTD. Demographic information, MMSE, recording length, and results using the LOSO setting of all subjects from Sub-066 to Sub-088. The average in the last line applies to all subjects in the two tables, from Sub-001 to Sub-088.

Subject ID	Gender	Age	Class	MMSE	Length	Sample-level Accuracy	Subject-level Accuracy
Sub-066	M	73	FTD	20	0.22h	67.17%	✓
Sub-067	M	66	FTD	24	0.28h	97.35%	✓
Sub-068	M	78	FTD	25	0.22h	26.06%	✗
Sub-069	M	70	FTD	22	0.31h	97.36%	✓
Sub-070	F	67	FTD	22	0.25h	68.77%	✓
Sub-071	M	62	FTD	20	0.31h	46.27%	✓
Sub-072	M	65	FTD	18	0.28h	50.94%	✓
Sub-073	F	57	FTD	22	0.39h	87.97%	✓
Sub-074	F	53	FTD	20	0.37h	94.46%	✓
Sub-075	F	71	FTD	22	0.31h	73.04%	✓
Sub-076	M	44	FTD	24	0.35h	77.96%	✓
Sub-077	M	61	FTD	22	0.27h	94.68%	✓
Sub-078	M	62	FTD	22	0.34h	90.94%	✓
Sub-079	F	60	FTD	18	0.25h	98.09%	✓
Sub-080	F	71	FTD	20	0.28h	94.20%	✓
Sub-081	F	61	FTD	18	0.25h	64.80%	✓
Sub-082	M	63	FTD	27	0.24h	65.38%	✓
Sub-083	F	68	FTD	20	0.27h	58.15%	✗
Sub-084	F	71	FTD	24	0.20h	15.91%	✗
Sub-085	M	64	FTD	26	0.18h	50.53%	✓
Sub-086	M	49	FTD	26	0.18h	20.11%	✗
Sub-087	M	73	FTD	24	0.19h	88.01%	✓
Sub-088	M	55	FTD	24	0.25h	68.81%	✓
Average	–	66.17	–	22.94	0.30h	79.74%	94.32%